

# DIFFRACTIVE PHENOMENA IN HIGH ENERGY PROCESSES

L. Frankfurt, Tel Aviv University, Tel Aviv, 69978, Israel  
leonidfrankfurt@gmail.com

M. Strikman

The Pennsylvania State University, University Park, PA, 16802, U.S.A.  
strikman@phys.psu.edu

October 29, 2018

## Abstract

We review the evolution of the studies of diffractive processes in the strong interaction over the last 60 years. First, we briefly outline the early developments of the theory based on analyticity and unitarity of the  $S$ -matrix, including the derivation and exploration of the Regge trajectories and related moving cuts. Special attention is paid to the concept of the Pomeron trajectory introduced for description of total, elastic and diffractive cross sections at high energies and to the emergence of the dynamics of multi-Pomeron interactions. The role of large longitudinal distances and color coherent phenomena for the understanding of inelastic diffraction in hadron–hadron scattering and deep inelastic scattering is emphasized. The connection of these phenomena to the cancellation of the contribution of the Glauber approximation in hadron–nucleus collisions and to the understanding of the Gribov–Glauber approximation is explained. The presence of different scales in perturbative QCD due to masses of heavy quarks has led to the emergence of numerous new phenomena including non-universality of the slopes of Regge trajectories made of light and heavy quarks and non-universal energy dependence of elastic cross sections. The application of the perturbative QCD techniques allowed us to calculate from the first principles the interaction of small transverse

size color singlets with hadrons leading to the development of the quantitative theory of hard exclusive reactions and to the successful prediction of many regularities in hard large mass diffraction. It also led to the prediction of the phenomenon of complete transparency of nuclear matter in QCD in special processes. The conflict of perturbative QCD with probability conservation for high energy processes of virtual photon–nucleon scattering is explained. Some properties of the new QCD regime are outlined.

## 1 Introduction

The aim of this chapter is to demonstrate that the phenomenon of diffraction in quantum chromodynamics (QCD) is a formative playground for the fundamental ideas and methods of theoretical physics. The deep disappointment of scientific society in the quantum field theory paradigm formulated by L. D. Landau at the Rochester Kiev conference (1959) [1] was based on the zero-charge problem in pre-QCD quantum field theories. As a result, the concept of the scattering matrix ( $S$ -matrix), where all quantities are in principle observable, became popular and replaced studies within the quantum field theory framework. The idea was that unitarity of the  $S$ -matrix, its analytic properties and exact symmetries will allow one to avoid dealing with point-like interactions characteristic for a quantum field theory such that the need for the ugly procedure of renormalization with all its puzzles will disappear. This approach led to the development of such new concepts as single and double dispersion relations, Regge trajectories, the Pomeron calculus, string models, etc and to the prediction of new phenomena. The discovery of asymptotic freedom in QCD in the late sixties to early seventies justified the space–time description of high energy processes in QCD, which is absent within the  $S$ -matrix concept. The account of the space–time evolution of high energy processes allowed one to predict a variety of striking new QCD phenomena such as color fluctuations, complete transparency of nuclear matter under special kinematic conditions, formation of a new QCD regime of the maximally strong interaction, etc., all of which are absent in the  $S$ -matrix theory. In the first part of this chapter, we consider the phenomenon of diffraction in the  $S$ -matrix theory and then discuss new diffractive phenomena that emerge in QCD studies.

The basic ideas of the  $S$ -matrix approach are unitarity of the  $S$ -matrix

in all physical channels and analyticity of scattering amplitudes in the complex planes of energies and momentum transfers that leads to analyticity of amplitudes in the plane of the angular momentum. The  $S$ -matrix approach justifies the concept of Regge trajectories. The assumption of the dominance of amplitudes of high energy processes by the Pomeron trajectory exchange predicts an increase with energy in the radius of the interacting hadron (shrinking with energy of the forward peak in two-body exclusive processes) and, therefore, the dominance of peripheral collisions, the universal dependence on energy of the total and elastic cross sections and cross sections of diffractive processes. The very existence of Pomeron moving cuts follows from unitarity of the  $S$ -matrix in the crossed channel. The prediction and experimental discovery of the large mass ( $M^2 \gg m^2$ ) triple Pomeron diffraction proves the non-zero value of the effective triple Pomeron interaction.

The modeling of the contribution of Pomeron moving cuts found blackening of interactions at central impact parameters since the contribution of the single Pomeron exchange grows with energy. However, the fraction of the total cross section due to the elastic scattering slowly grows with energy. For the current LHC energy:

$$\sigma_{\text{elastic}}(pp)/\sigma_{\text{tot}}(pp) \approx 0.25. \quad (1)$$

Thus, the  $pp$  interaction is still very far from the regime of complete absorption where this ratio should be close to 0.5. Note, however, that for the central  $pp$  collisions, almost complete absorption has been observed at Fermi National Accelerator Laboratory (FNAL) and the LHC, which corresponds to partial amplitudes being close to unity. Thus an energetic proton, when interacting with the proton target, behaves as a grey disc with a black spot in the center. The size of the black spot rapidly increases with energy.

The assumption that the amplitudes of high energy hadron-hadron collisions depend on one scale was challenged by the discovery of  $J/\psi$ ,  $\Upsilon$  mesons – bound states of heavy quarks:  $c\bar{c}$  and  $b\bar{b}$ . The radii of these quarkonia states are significantly smaller than for hadrons made of light quarks. The interaction of  $Q\bar{Q}$  quarkonia with hadrons made of light quarks is decreasing with  $m_Q$  in the non-perturbative and perturbative QCD domains.

Analyses of the ladder diagrams for cross sections of deep inelastic scattering off a hadron target found that longitudinal distances dominating in the scattering process are linearly increasing with energy in QCD. As a result, at sufficiently large energies they exceed by far the length of the target,

the transitions between different configurations in the projectile slow down and the interaction can be described as a superposition of the interaction of instant quark–gluon configurations within the projectile. This feature leads to the fluctuations of strengths of hadron–hadron and hadron–nucleus interactions and to the exact cancellation of the Glauber model contribution to hadron (nucleus)–nucleus collisions. This cancellation follows directly from the analytic properties of amplitudes and/or energy–momentum conservation. The Gribov–Glauber model replaces the Glauber model in high energy processes where diffraction is a shadow of inelastic processes.

The fluctuations of strengths of the interaction in hadron–hadron collisions found an explanation in QCD as being due to the color screening phenomenon. The fluctuations of strengths of the interaction within the virtual photon wave function have been observed directly in the significant cross section of leading twist diffraction in deep inelastic scattering (DIS), which is predicted to be negligible in perturbative QCD (pQCD) because of the absence of free quarks and gluons. However, it was observed in  $ep$  DIS at HERA that the cross section of diffractive processes constitutes  $\approx 10\%$  of the total cross section at  $x \approx 10^{-3}$  and the ratio of the diffraction cross section to the total one is practically energy, and  $Q^2$  - independent ( $Q^2$  is the photon virtuality).

QCD dynamics predicts the existence of hard diffractive phenomena that are higher twist effects. The significant difference in momentum scales characterizing hard and soft (non-perturbative) processes allows one to prove the factorization of hard processes from soft ones and to calculate cross sections of hard diffractive processes. The processes of elastic photoproduction of mesons with hidden heavy flavors off the proton target and elastic electroproduction of light mesons observed at HERA revealed an interplay of the dependence of the cross sections on energy, the photon virtuality  $Q^2$ , and the momentum transfer  $t$  that is close to that expected in pQCD.

Diffraction in high energy processes is a shadow of inelastic processes so that, for sufficiently small  $x$ , an increase with energy of the structure functions of nucleons and nuclei, which is predicted in pQCD approximations, runs into conflict with the probability conservation at small impact parameters. The range of central impact parameters, where the regime of complete absorption dominates, increases with an increase of energy (for fixed  $Q^2$ ). In this regime at ultrahigh energies,  $\sigma(pp) \propto \ln^2(s/s_0)$  and  $\sigma(\gamma^*p) \propto \ln^3(s/s_0)$ . The complete absorption regime is possibly reached for the gluon distribution at the central impact parameters and at  $Q^2$  of the order of a few  $\text{GeV}^2$

in electron–proton collisions at HERA. Physics related to the formation of strong gluon fields at sufficiently small  $x \approx Q^2/s$  and small impact parameters can be probed at the LHC and Large Hadron–Electron Collider (LHeC). In this new QCD regime the expansion over powers of  $1/Q^2$  (twists) becomes meaningless. Also, there arises the question whether continuous symmetries such as conformal and scale invariances characterizing pQCD and new QCD regimes are different.

No significant violation of the Dokshitzer–Gribov–Lipatov–Altarelli–Parisi (DGLAP) approximation for the structure functions integrated over impact parameters is predicted at achieved  $x$ . This is because the structure functions are dominated by the scattering at the impact parameters growing with energy where the interaction remains weak even though it reaches the black limit at the central impact parameters. Moreover, no noticeable slowing down of an increase of the structure functions with energy is expected at even smaller  $x$  since the black limit contribution rapidly increases with a decrease in  $x$  at the energies achievable in laboratory.

It was suggested to sum the leading  $\alpha_s \ln(x_0/x)$  terms in the kinematics of fixed  $Q^2$  and  $x \rightarrow 0$  – leading logarithmic (LL) approximation. There were derived formulas for the collision of two small size ( $\approx 1/Q$ ) wave packets,  $\gamma^*(Q^2) + \gamma^*(Q^2) \rightarrow X$ , in which case the diffusion in the  $k_t$  space is suppressed (which may work for limited range of energies). The same formulas are often applied to the scattering of a small size ( $\approx 1/Q$ ) wave packet ( $\gamma^*$ ) off the proton target that has a size of  $\approx 1/(2m_\pi)$ . In this case the neglected within the LL approximation diffusion to small parton momenta within the parton ladder is rather important. Energy and momentum of the final states calculated within the leading log approaches are significantly different from that for initial state especially within the leading  $\alpha_s \ln(x_0/x)$  approximation. This violation follows from the choice of the kinematical domain characteristic for LL approximation. Conservation of energy-momentum is guaranteed after resummation over series of LO, NLO, NNLO... approximations. This property of approximation explains negative sign and huge value of next-to-leading order (NLO) ”corrections” and requires the development of resummation approaches. However, diffractive processes were not considered yet in the resummation approaches.

The chapter is organized as follows. In section 2 we define the kinematics characteristic for diffractive phenomena in hadronic collisions and briefly review the  $S$ -matrix approach: analytic properties of amplitudes of high energy processes in the energy, momentum transfer and orbital momentum

planes. We also explain how the concept of Regge trajectories in the angular momentum plane arises in the relativistic theory of the scattering matrix.

In section 3, we remind basic properties of Regge trajectories and explain that the linearity and universality of Regge pole trajectories is confirmed by comparison of Regge trajectories with the data on hadron resonances made of light  $u$ ,  $d$ , and  $s$  quarks. This linearity and the assumption that the amplitude is dominated by the Regge pole trajectory exchange allows one to reproduce the observed dependence of cross sections of two-body processes with non-vacuum quantum numbers in the crossed channel on energy. We also explain that the assumption that all Regge trajectories have the same universal slope does not hold for the trajectories with hidden and open heavy flavors. It contradicts the quarkonium models and the data. We also explain how moving cuts accompanying the Regge pole follow from the unitarity of the  $S$ -matrix in the plane of angular momentum.

In section 4, we consider the hypothesis that the dominant exchange in the amplitudes of high energy processes, is the one by the Pomeron trajectory accompanied by Pomeron moving cuts—Pomeron calculus. The dominance of peripheral collisions and the important role of Gribov diffusion in the impact parameter space are explained. A brief comparison with data shows that such predicted basic features of high energy processes as the universal energy dependence of all high energy processes and the shrinking with energy of the diffractive peak agree with the data. We discuss properties of multi-Pomeron interactions, the evidence for triple Pomeron interactions and their role in diffraction at the Tevatron and LHC. The impact of multiple rescatterings of Pomerons on the elastic differential cross section is also briefly discussed.

In the framework of the Pomeron calculus, we also explain an onset of the regime of the complete absorption at small impact parameters, some of its properties and compare it briefly with the selected FNAL and LHC data. Implications for the value of the slope of the Pomeron trajectory in the regime of complete absorption at small impact parameters are briefly discussed.

In section 5 the space–time evolution of high energy processes and the linear increase with energy in longitudinal distances in the scattering process are discussed. As a result, the contribution of planar diagrams—known as the Glauber model for hadron–nucleus collisions—is cancelled out. Moreover the contribution of the planar diagrams (the Glauber approximation) violates energy-momentum conservation.

At the same time, the contribution of non-planar diagrams can be rewritten in the form of the Glauber approximation but with an additional inelastic

shadowing term—the Gribov–Glauber model.

In section 6 we explain that in QCD, the increase of longitudinal distances with the collision energy leads to a variety of coherent phenomena which we refer to as the color fluctuation phenomena. They include the presence of inelastic diffraction at the zero angle and the processes where hadrons fluctuate into small - size configurations and interact with the small strength so that nuclei do not absorb them—color transparency (CT). CT allows one to prove QCD factorization theorems for a number of processes. At the same time, the concept of color fluctuations allows us to bridge the gap between the fluctuations to small- and large-size configurations and to reconstruct the distribution over cross sections for projectile hadrons and photons. It also gives us a physically transparent interpretation of the Gribov–Glauber model that could be applied to modeling proton (nucleus)–nucleus collisions. The concept of color fluctuations allows us to build the QCD-improved aligned jet model. The significant cross section of diffraction in deep inelastic small  $x$  processes observed at HERA, its  $Q^2$  and energy dependencies are direct confirmation of the important role of color fluctuations in high energy processes. We also briefly review the concept of the perturbative Pomeron in pQCD.

In section 7, we explain the QCD factorization theorem for hard exclusive processes, derive basic characteristics of hard diffractive processes and briefly compare the derived formulas with the data obtained at FNAL and HERA. We point out that complete transparency of nuclear matter for special hard diffractive processes has been predicted and confirmed by the FNAL data.

In section 8, we discuss the onset of the new QCD regime and its basic features in the limit of fixed  $Q^2$  and  $x \rightarrow 0$ . The conflict between pQCD calculations and probability conservation in the collisions at central impact parameters, the onset of the black disc regime (BDR), and competition between the soft QCD and pQCD contributions are explained.

Conclusions are presented in section 9 .

## 2 General properties of the scattering amplitude

### 2.1 Kinematics

We consider first the scattering of two particles:

$$a + b \rightarrow a + b. \quad (2)$$

The amplitude of this process depends on the four-momenta of the colliding particles  $p_i$ . An account of energy–momentum conservation gives the constraint:

$$p_a + p_b = p'_a + p'_b. \quad (3)$$

Lorentz invariance restricts the number of independent variables. The convenient variables are the square of the energy in the  $s$ -channel center of mass:  $s = (p_a + p_b)^2$ , and the squares of the momentum transfer between  $a$  and  $a'$   $t = (p_a - p'_a)^2$ , and between  $a$  and  $b'$ :  $u = (p_a - p'_b)^2$ . These three variables are not independent. Energy–momentum conservation (Eq. 3) leads to

$$s + t + u = 2[m_a^2 + m_b^2]. \quad (4)$$

If the scattered particles are the lowest-mass states in the channels with given quantum numbers, there exist three physical channels where the scattering process is allowed:  $s \geq (m_a + m_b)^2$ ,  $(t, u) \leq 0$ ;  $t \geq \max\{4m_a^2, 4m_b^2\}$ ,  $(s, u) \leq 0$ ;  $u \geq (m_a + m_b)^2$ ,  $(t, s) \leq 0$ . Thus the physical meaning of the variables  $s$ ,  $t$  and  $u$  is that each of them is equal to square of the center-of-mass energy of colliding particles in the corresponding center of mass of the physical channel:  $a$  and  $b$  in the  $s$ -channel,  $a$  and  $\bar{a}$  in the  $t$ -channel and  $a$  and  $\bar{b}$  in the  $u$ -channel. The amplitudes in all three channels are interrelated by rotation of the four-momenta of the particles.

### 2.2 S-matrix approach

Before the advent of quarks and later QCD the most important ideas of the theory of strong interactions were suggested within the concept of the scattering matrix,  $S$ . The matrix elements of the  $S$ -matrix describe amplitudes of the scattering processes where hadrons in the initial and final states are



outside the interaction region. In the physical region of any physical process, the  $S$ -matrix is restricted by its unitarity, i.e., by probability conservation:

$$SS^\dagger = 1. \quad (5)$$

To single out the contribution when no interaction occurs, the  $T$ -matrix is introduced:  $S = 1 + iT$ . The unitarity condition for the  $T$ -matrix has the following form in the  $s$ -channel:

$$\text{Im} T(a + b \rightarrow a + b) = \frac{1}{2} \int \sum_n \langle a + b | T | n \rangle d\tau_n \langle n | T | a + b \rangle^\dagger, \quad (6)$$

where  $d\tau_n$  is the phase volume for the state  $n$ . The above equation can be rewritten as the optical theorem which relates  $T$  matrix with the total cross section:

$$\text{Im} T(a + b \rightarrow a + b) = s \sigma_{\text{tot}}(a + b), \quad (7)$$

where  $s = (p_a + p_b)^2$ .

The hope was that in a relativistic theory, the conservation of probability, i.e., the  $S$ -matrix unitarity (Eq. 5), and threshold singularities in the crossed channel would substitute the non-relativistic concept of the potential.

### 2.3 Brief summary of analytic properties of amplitudes in energy, momentum and orbital momentum planes

The aim of this subsection is to briefly remind of basic ideas and results obtained in the  $S$ -matrix approach.

One starts with imposing causality in the form of the Lehman, Symanzic and Zimmermann (LSZ) representation of the amplitude as the Fourier transform of the matrix elements of the retarded commutator of currents [2]. This leads to the assumption that the amplitudes of the physical processes are the boundary values of the same analytic function of the energy and momentum transfers. The singularities of the amplitudes are given by the thresholds for the physical processes [3], see the discussion below.

S. Mandelstam proposed the double dispersion representation which takes into account the singularities both in the momentum transfer and in the energy planes [4]:

$$A(s, t) = \frac{1}{\pi^2} \int_{4m^2}^{\infty} ds' dt' \frac{\rho_{st}(s', t')}{(s' - s)(t' - t)} + \frac{1}{\pi^2} \int_{4m^2}^{\infty} du' dt' \frac{\rho_{ut}(u', t')}{(u' - u)(t' - t)} \quad (8)$$

$$+\frac{1}{\pi^2} \int_{4m^2}^{\infty} du' dt' \frac{\rho_{su}(s', u')}{(s' - s)(u' - u)},$$

where we take  $m_a = m_b$  for simplicity. All denominators are understood as having imaginary parts:  $(s' - s)^{-1} = (s' - s - i\epsilon)^{-1}$ . (This condition selects the outgoing wave.) In the following we will not need the exact form of the spectral densities  $\rho_{i,j}$  which were supposed to follow from unitarity of the  $S$ -matrix and its analytic properties [5].

Dispersion representations over the variables  $s$  and  $t$  follow directly from the double dispersion representation. Also, they can be derived directly from the theoretical analysis of the LSZ representation of the scattering amplitude, see the discussion and references in [6]. The dispersion representation of the scattering amplitude in the energy plane is:

$$A(s, t) = \frac{1}{\pi} \int_{4m^2}^{\infty} ds' \frac{Im_s A(s', t)}{s' - s} + \frac{1}{\pi} \int_{4m^2}^{\infty} du' \frac{Im_u A(u', t)}{u' - u} + \text{subtractions}. \quad (9)$$

By definition subtractions do not have imaginary part in variables  $s$  and  $u$ . It follows from unitarity of the  $S$ -matrix and analyticity that in the physical region, the scattering amplitudes at large energies are restricted by the condition:  $ImA \leq cs \ln^2(s/s_o)$  [7]. For the amplitude symmetric under the transformation  $s \rightarrow u$ , the subtraction term is constant. For the amplitude antisymmetric under the transformation  $s \rightarrow u$  (negative signature), the subtraction term is  $\propto s$ .

The dispersion representation over the momentum transfer  $t$  has a similar form:

$$A(s, t) = \frac{1}{\pi} \int_{4m^2}^{\infty} du' \frac{Im_u A(u', t)}{u' - u} + \frac{1}{\pi} \int_{4m^2}^{\infty} dt' \frac{Im_t A(t', s)}{t' - t} + \text{subtractions}. \quad (10)$$

Emergence of the concept of Regge poles in the relativistic theory was enabled by the combination of Eq. 8 for the analytic continuation of the decomposition of the scattering amplitudes over partial waves to the crossed channel with the  $S$ -matrix unitarity condition in the crossed  $t$ -channel.

One starts with the observation that the  $S$ -matrix unitarity condition becomes diagonal if the conservation of the angular momentum is taken into account. Hence it is convenient to decompose the amplitude over partial waves:

$$A(s, t) = 8\pi \sum_l f_l(s) (2l + 1) P_l(z), \quad (11)$$

where  $z = 1 + 2t/(s - 4m^2)$ ;  $P_l(z)$  are the Legendre polynomials. For simplicity, we consider collisions of hadrons with spin zero. (A generalization to the case of scattering of particles with non zero spin is straightforward but would make formulae unnecessary lengthy.)

$$f_l(s) = \frac{1}{2} \int_{-1}^1 dz P_l(z) \frac{A(s, t)}{8\pi}. \quad (12)$$

The normalization of  $f_l$  is chosen so that unitarity of the  $S$ -matrix has the form:

$$\text{Im} f_l(s) = \frac{1}{2} f_l(s) f_l^*(s) + \text{positive terms}. \quad (13)$$

In high energy processes, orbital momenta essential in the scattering process are large. Hence it is legitimate to substitute the sum over the orbital momenta  $l$  by the integral over the impact parameters  $b$ ,  $l + 1/2 = pb$ , where  $p$  is the center of mass momentum. (The factor of  $1/2$  follows from the necessity to reproduce the formulae of the semi-classical approximation in non-relativistic quantum mechanics.) At large energies,  $p \approx \sqrt{s}/2$ . Thus we derive the impact parameter representation of the amplitude:

$$A(s, t) = 4\pi s \int db b f(b, s) J_0(q_t b) = (2s) \int d^2\vec{b} \exp(i\vec{q}_t \cdot \vec{b}) f(b, s), \quad (14)$$

where  $q_t = p \sin(\theta)$  and  $\theta$  is the c.m. scattering angle. In the derivation we used the asymptotic expression for the Legendre polynomials at large  $l$ :  $P_l(\theta) \approx J_0((l + 1/2)\theta)$  and the integral representation of the Bessel function  $J_0$ :  $J_0(q) = (1/2\pi) \int_0^{2\pi} \exp(iq \cos(\phi)) d\phi$ .

We can use the dispersion representation of the amplitude over the momentum transfer and properties of the Legendre functions of the second kind to derive the representation that can be easily continued into the complex plane of the orbital momentum:

$$f_l(s) = \frac{1}{2\pi i} \int_C \frac{Q_l(z) A(t, z)}{8\pi} dz. \quad (15)$$

Here the contour of integration encircles the  $[-1, 1]$  interval on the real axis. The integrand has singularities outside the contour at

$$z_1 = 1 - ((4m^2)/(s - 4m^2)), \quad z_2 = -1 + ((4m^2)/(s - 4m^2)), \quad (16)$$

corresponding to the singularities of the amplitude at  $t = 4m^2$  and  $u = 4m^2$ .

The Legendre functions of the second kind satisfy the relation:

$$Q_l(z) = \frac{1}{2} \int_{-1}^1 P_l(z') dz' / (z' - z). \quad (17)$$

The advantage of this function is that for  $z \gg 1$ :

$$Q_l(z) \propto \frac{1}{z^{l+1}}, \quad (18)$$

and that for  $-1 \leq z \leq 1$ ,

$$Q_l(z + i\epsilon) - Q_l(z - i\epsilon) = -i\pi P_l(z). \quad (19)$$

For the discussion in the next section, it is important to derive the representation of the partial wave in  $t$ -channel. For sufficiently large  $l$ , the integration contour in Eq. 15 can be deformed around the singularities of the amplitude since the integral over the large circle is equal to zero. Thus, another representation arises:

$$f_l(t) = \frac{1}{\pi} \int_{z_1}^{\infty} dz \frac{Q_l(z) A_t(z, s)}{8\pi} + (-1)^l \frac{1}{\pi} \int_{z_2}^{\infty} \frac{Q_l(z) A_t(z, u)}{8\pi} dz. \quad (20)$$

The presence of the factor of  $(-1)^l = \exp(i\pi l)$  precludes analytic continuation of the amplitude to the complex plane of the orbital momentum since the factor  $(-1)^l = \exp(i\pi l)$  increases rapidly with  $lm$ . To remove the factor of  $(-1)^l$ , it is convenient to introduce the functions  $f_l^\pm(t)$  which are symmetric and antisymmetric under the  $s \rightarrow u$  transposition, respectively—functions with the positive and negative signature. Thus,

$$f_l^\pm(t) = \frac{1}{\pi} \int_{z_1}^{\infty} \frac{Q_l(z) A_t(z, s)}{8\pi} \pm \frac{1}{\pi} \int_{z_2}^{\infty} \frac{Q_l(z) A_t(z, u)}{8\pi}, \quad (21)$$

which provides the analytic continuation of the partial waves to the complex plane of the angular momentum. Above formulae are known as the Gribov–Froissart projection [8].

## 3 Regge poles in the $S$ -matrix theory

### 3.1 Regge poles and $t$ -channel unitarity

T. Regge found in the non-relativistic quantum mechanics that the scattering amplitude in the unphysical region corresponding to large imaginary

scattering angles,  $\cos(\theta) \rightarrow \infty$ , has the following form:

$$A(s, t) \propto \cos(\theta)^{l(E)}, \quad (22)$$

where  $l(E)$  is the eigenvalue of the operator of the orbital momentum  $l$  at a given energy  $E$ . The eigenvalues of the energy  $E_n$  follow from the condition that  $l = n$ , where  $n$  is an integer number. Thus the concept of the Regge trajectory  $l(E)$  allows one to describe both the energy eigenstates and the asymptotic behavior of the amplitude [9]. In a relativistic theory, the  $s$ -channel  $\cos(\theta) \propto s$  and  $E$  should be substituted by  $t$ .

S. Mandelstam observed that in a relativistic theory, the kinematics of large  $s$  and fixed  $t \ll s$  corresponds to physical processes with  $s \gg 4m^2$  which are usually called the crossed channel with respect to the  $t$ -channel processes. As cited in [10], he suggested that the Regge pole behavior, would allow for a simple description of bound states. The key tool for the derivation of the basic properties of Regge trajectories and the calculation of the amplitudes of high energy processes is the partial amplitudes in the  $t$ -channel analytically continued to the complex plane of orbital momentum—the Gribov–Froissart projection discussed in the previous section. Regge trajectories describe the sum of poles of these amplitudes which follow from unitarity of the  $S$ -matrix in the crossed channel. The concept of the Regge trajectory  $l(t)$  is useful for the description of hadron resonances with the same quantum numbers (except for spin) and for the calculation of amplitudes of high energy processes.

Important properties of Regge trajectories follow from the two-particle  $t$ -channel unitarity condition continued to the angular momentum plane:

$$\frac{1}{2}(f_l^\pm(t + i\epsilon) - f_l^\pm(t - i\epsilon)) = (1/2)f_l^\pm(t + i\epsilon)f_l^\pm(t - i\epsilon), \quad (23)$$

which can be rewritten as

$$f_l^\pm(t) - f_l^{\pm*}(t) = f_l^\pm(t)f_l^{\pm*}(t). \quad (24)$$

In the proof one uses the observation that for  $t \leq 4m^2$ ,  $f^\pm$  are real and hence  $f^\pm(t - i\epsilon) = [f^\pm(t + i\epsilon)]^*$ . The two-particle  $t$ -channel unitarity condition is exact for  $4m^2 \leq t \leq 16m^2$  and allows one to prove the existence of Regge poles in relativistic amplitudes and to establish some of their properties [11, 12].

The Gribov–Froissart projection has pole at  $l = l(t)$ :

$$f_l(t) = c/(l - l(t)). \quad (25)$$

Taking into account the real and imaginary parts of the trajectory  $l(t)$ , it is easy to find out that in the vicinity of  $l$ , the amplitude is described by the Breit–Wigner formulas, see also [13]. Thus the concept of the Regge trajectory (which is often called the moving trajectory) describes hadronic resonances with the same quantum numbers, except for the spin.

Using these equations and iterating one Regge trajectory, it is easy to show that the Regge trajectory generates the moving pole singularities in the complex plane of the angular momentum  $l$  [12, 14].

### 3.2 Regge poles and high energy behavior of amplitudes of physical processes

To demonstrate the role of Regge poles in high energy processes in the relativistic theory, it is convenient to use the method applied by Sommerfeld to the problem of diffraction of radio waves around Earth. The task is to find an analytic function of  $l$  which coincides with  $f_l(t)$  for integer points  $l = 0, 1, 2, \dots$

The decomposition of the positive signature amplitude over partial waves in the  $t$ -channel diverges with an increase in  $s$  because the Legendre polynomials—being the functions of  $z = 1 + 2s/(t - 4m^2)$ —increase as powers of  $s$ :

$$P_l(\cosh(\alpha))_{l \rightarrow \infty} \propto \frac{\exp^{(l+1/2)\alpha}}{\sqrt{2\pi \sin(\alpha)}}. \quad (26)$$

The partial amplitudes are restricted by the  $S$ -matrix unitarity and their imaginary parts are positive. Thus one needs to continue partial waves analytically to the angular momentum plane. The procedure was explained in the previous section.

The first step is to identically represent the amplitude as a contour integral over the orbital momenta  $l \geq 0$  around the real axis:

$$A^+(s, t) = (1/i) \int_C dl \xi_l^+(t) f_l^+(t) (2l + 1) P_l(1 + 2s/(t - 4m^2)), \quad (27)$$

where  $\xi_l^+(t)$  is called the positive signature factor. It can be written as

$$\xi_l^+(t) = [1 + (-1)^{i\pi l}] / \sin(\pi l) = \exp i(\pi l/2) / \sin(\pi l/2). \quad (28)$$

Taking the residues over the poles of  $1/\sin(\pi l/2)$  would recover Eq. 11.

For the amplitude antisymmetric with respect to the transposition  $s \rightarrow u$ , the signature factor is:

$$\xi_-(l) = \exp i(\pi l/2) / \cos(\pi l/2). \quad (29)$$

It follows from the location of singularities in the plane of  $t$  that  $f_l(t) \propto \exp(-\mu l)$  for  $l \rightarrow \infty$ , where  $\mu$  is the minimal mass in the singularities over  $t$ . Hence, for the integration contour  $C$ , one can take the straight line between the points  $l_0 - i\infty$  and  $l_0 + i\infty$ . The contour can be moved to the left until it encounters singularities of the amplitudes in  $l$  that do not allow further shifting of the counter to the left. In this discussion,  $l_0 \geq -2$  since the positive signature amplitude cannot decrease with  $s$  faster than  $1/s^2$ . This property follows from the fact that imaginary part of this amplitude is always positive. In addition, one should take into account poles and cuts in the  $l$ -plane. Thus, the expression for the positive signature amplitude reads:

$$A^+(s, t) = (1/i) \int_{l_0 - i\infty}^{l_0 + i\infty} dl \xi^+(l) f_l^+(t) (2l + 1) P_l(1 + 2s/(t - 4m^2)) + \Delta, \quad (30)$$

where  $\Delta$  is the contribution of the Regge poles and moving cuts. A similar analysis can be performed for the negative signature amplitude.

The contribution of the Regge pole  $f_l(t) \propto 1/(l - \alpha(t))$  to the amplitude  $A$  has the form:

$$g_{a,a'}(t) g_{b,b'}(t) (s/s_0)^{\alpha(t)} \xi(t). \quad (31)$$

Factorization of the dependence of the amplitude on the properties of the particles  $a$  and  $b$  follows from the unitarity condition for the partial waves in the  $t$ -channel [12].

V. Gribov has demonstrated [15] that the textbook models that assume that the total cross section of hadronic collisions at large  $s$  is energy independent and the  $t$  dependence of the elastic amplitude does not depend on  $s$ , i.e.,  $A(s, t) = i s f(t)$ , are incompatible with probability conservation in the crossed channel as given by Eq. 24. Such a behavior corresponds to the fixed pole in the orbital momentum plane. However, a single pole  $1/(l - 1)$  on the left-hand side of this equation cannot be equal to a double pole  $1/(l - 1)^2$  on the right-hand side of it.

Common wisdom based on the  $S$ -matrix approach was that any hadron is a bound state of other hadrons but not of some elementary constituents. This concept was implemented by assuming that hadrons belong to Regge

trajectories. In quantum chromodynamics, hadrons are bound states of elementary particles—quarks and gluons—and physical states contain no free quarks and gluons (the hypothesis of confinement of quarks and gluons). This makes the Regge trajectory description of hadrons even more plausible.

### 3.3 Regge trajectories

G. Chew and S. Frautchi suggested to describe the spectrum of hadrons in terms of the Regge pole trajectories [13]. The mass of a hadron follows from the equation:

$$\alpha(t_h) = J_h, \quad (32)$$

where  $J_h$  is the spin of the resonance and  $t_h$  its mass. The scattering amplitude has poles for these values of  $l$  and  $t$ .

The observed spectrum of hadrons made of light quarks as well as cross sections of exclusive processes with non-vacuum quantum numbers in the crossed channel are well described by the Regge trajectories linear in the momentum transfer  $t$  [13]:

$$\alpha(t) = \alpha_0 + \alpha' t. \quad (33)$$

The data prefer practically the same slope  $\alpha'$  for all hadrons made of the light  $u$ ,  $d$ , and  $s$  quarks:

$$\alpha' \approx 1 \text{ GeV}^{-2}. \quad (34)$$

The values of the intercept  $\alpha_0$  for the leading trajectories are the following:

$$\alpha_\rho(t=0) \approx 0.5, \quad \alpha_{A_2}(t=0) \approx 0.3, \quad \alpha_\pi(t=0) \approx 0. \quad (35)$$

For completeness, we also enumerate other important results which, however, we will not use in this chapter:

(i) An analysis of the experimental data on meson resonances and exclusive processes indicates that the meson trajectories with positive and negative signatures are close, see [16] for a review and references.

(ii) Fermion trajectories should also contain the term  $\propto \sqrt{t}$ , otherwise the trajectories with opposite signatures will be degenerate [17]. However, the data on two body processes dominated by fermion exchanges are very limited.

(iii) There has been proposed a technique of calculation of the corresponding QED amplitudes in the angular momentum plane [18] which allows to



establish whether constituents of QED belong to moving Regge pole trajectories. A more powerful technique of identifying and calculating the leading Feynman diagrams in a quantum field theory containing vector particles has been developed in [17].

(iv) It has been shown that in non-abelian gauge theories massive vector mesons [19] and fermions [20] are reggeized in the perturbative regime. In QCD the presence of infrared singularities related to the zero mass of the gluon requires to take into account addition infrared factor.

(v) It has been observed that the sum of  $s$ -channel resonances produces linear Regge trajectories in the  $t$ -channel [21]. This hypothesis is the basis of string models.

The knowledge of Regge trajectories allows one to predict cross sections of two-body high energy processes with non-vacuum quantum numbers in the crossed channel.

### 3.4 Regge pole theory for non-vacuum exchanges

It has been suggested that reactions with non-vacuum quantum numbers in the crossed channel are dominated at high energies by the exchange of the Regge trajectories allowed by conservation of charge, spatial parity, G-parity and isotopic spin [22].

Assuming the dominance of the Regge pole contribution to the amplitude of diffractive processes, one obtains:

$$\begin{aligned}
\frac{d\sigma(a + b \rightarrow a' + b')}{dt} &= \frac{g_{aRa'}^2(t)g_{bRb'}^2(t)}{\sin^2(\pi\alpha_R(t)/2)} \left(\frac{s}{s_0}\right)^{2(\alpha_R(t)-1)} \\
&+ \frac{g_{aR'a'}^2(t)g_{bR'b'}^2(t)}{\cos^2(\pi\alpha_{R'}(t)/2)} \left(\frac{s}{s_0}\right)^{2(\alpha_{R'}(t)-1)} \\
&+ 2 \frac{g_{aRa'}(t)g_{bRb'}(t)}{\sin(\pi\alpha_R(t)/2)} \frac{g_{aR'a'}(t)g_{bR'b'}(t)}{\cos(\pi\alpha_{R'}(t)/2)} \left(\frac{s}{s_0}\right)^{(\alpha_R(t)+\alpha_{R'}(t)-2)} \\
&\times \cos((\pi/2)(\alpha_R - \alpha_{R'})). \tag{36}
\end{aligned}$$

This expression takes into account the exchanges of the trajectories with positive ( $R$ ) and negative ( $R'$ ) signatures. Fitting Regge trajectories as a linear function of  $t$  gives a good description of the mass spectrum of the resonances belonging to the corresponding trajectories (see, e.g. Fig. 1). The

assumption that the trajectories remain linear for  $t \leq 0$  leads to a reasonable description of the data using Eq. 36.

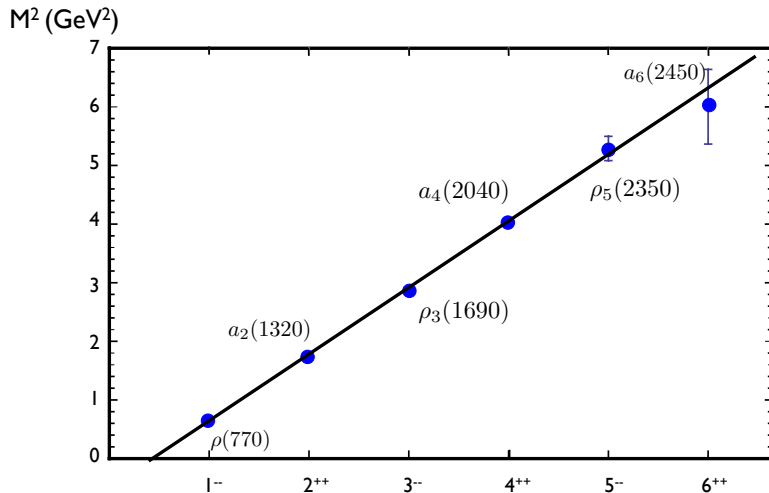


Figure 1: The lowest mass mesons lying on the  $\rho$  Regge trajectory and on the nearly degenerate  $A_2$  trajectory.

The data exist for the cross sections of the following processes (see the review [16]):  $\pi^- + p \rightarrow \pi^0 + n$ ,  $\pi^- + p \rightarrow \rho(A_2) + n$ ,  $K^- + p \rightarrow \phi + n$ ,  $p + p \rightarrow \Delta + N$ , etc. These data are described well at small  $t$  by the exchange of a few leading Regge meson trajectories. In the kinematics of large  $s$  and small  $u$ , the exchange of the baryon trajectories dominate such processes as, e.g.,  $\pi^- + p \rightarrow p + \pi^-$ . The data are described well in terms of linear meson and baryon trajectories for  $-t \leq 0.5 \text{ GeV}^2$  (see, e.g., the review [16]). At the same time, for  $-t \geq 1 \text{ GeV}^2$  data can be interpreted as the evidence for flattening of meson and baryon trajectories to the values corresponding to the exchange of reggeized  $q\bar{q}$  ( $qqq$ ) systems [23]. Further experimental studies of high energy two-body reactions in the  $-t = \text{const} \geq 1 \text{ GeV}^2$  limit would be highly desirable.

### 3.5 Non-universality of the Regge trajectories for the bound states containing heavy quarks

The states containing heavy quarks belong to the Regge trajectories with the slope different from the one of the Regge trajectories for hadrons made of light quarks. We will give here two examples.

(i) In the  $M_Q \rightarrow \infty$  limit, the masses of  $Q\bar{q}$  states are  $M_{Q\bar{q}}(n) = M_Q + \Delta_n$ , where  $\Delta_n$  are independent of  $M_Q$ . This result follows from quarkonium models and is probably valid in QCD. Therefore, for linear trajectories one has:

$$\alpha'_{Q\bar{q}} \approx \frac{1}{2M_Q(\Delta_1 - \Delta_0)}. \quad (37)$$

This slope is different from the universal slope suggested in the string models for a hadron trajectory consisting of light quarks.

(ii) For hadrons with hidden flavor, the slope of the  $Q\bar{Q}$  trajectory decreases with the mass of the heavy quark in the  $M_Q \rightarrow \infty$  limit as:

$$\alpha'_{Q\bar{Q}} \propto \frac{1}{\alpha_s^2 M_Q^2}. \quad (38)$$

For an estimate, we used here quarkonium models with the Coulomb interaction between quarks.

To conclude, the large masses of heavy quarks supply extra scales in addition to the  $\Lambda_{QCD}$  scale, which suggests the existence of a variety of phenomena beyond the framework of the one-scale  $S$ -matrix theory [24]. For example,  $J/\psi$  and  $\Upsilon$  have significantly smaller radii than the pion:

$$r_\pi = 0.5 \text{ fm}, \quad r_{J/\psi} \approx 0.2 \text{ fm}, \quad r_\Upsilon \approx 0.1 \text{ fm}. \quad (39)$$

As a consequence of color screening and asymptotic freedom, heavy quarkonia relatively weakly interact with hadrons made of light quarks. (The probability of the pion field around a heavy quarkonium in the ground state is close to zero.) The observed total and partial widths and the cross section of diffractive photoproduction of  $J/\psi$  at moderate energies are significantly smaller than those for vector mesons made of light quarks.

## 4 Pomeron theory of high energy soft QCD processes

### 4.1 Introducing the concept of the Pomeron exchange

We discuss briefly here the hypothesis of the Pomeron exchange dominance in the amplitudes of high energy processes.

The Pomeranchuk theorem,

$$\sigma(h + T) = \sigma(\bar{h} + T), \quad (40)$$

was proven initially under the assumption that  $\sigma_{\text{tot}}(hN) \rightarrow \text{const}$  for  $s \rightarrow \infty$ . The proof uses analytic properties of amplitudes in the energy plane and that the amplitude is predominantly imaginary at high energies. Indeed,  $A^+(s, t) = c^+[s \ln(-s) + u \ln(-u)] \approx ic^+\pi s$  which should be compared with  $A^- = c^-[s \ln(-s) - u \ln(-u)] \approx 2c^-s \ln(-s)$ . The condition:  $A^+ \gg A^-$  requires that  $c^- = 0$ —the Pomeranchuk theorem [25]. In the more realistic case of a growing cross section, a weaker form of the theorem for  $s \rightarrow \infty$  can be proven:

$$\sigma_{\text{tot}}(h + T)/\sigma_{\text{tot}}(\bar{h} + T) \rightarrow 1. \quad (41)$$

This theorem is confirmed by the data on  $\sigma_{\text{tot}}(pp)$  and  $\sigma_{\text{tot}}(p\bar{p})$ .

As we explained in section 3.2, the behavior of the scattering amplitude  $A(s, t) = isf(t)$ , which is typical for quantum mechanical problems with the absorptive interaction, contradicts the  $S$ -matrix unitarity relation for partial waves in the crossed  $t$ -channel. To resolve this contradiction, V. Gribov [15] suggested the behavior of the scattering amplitude (for large  $s$  and small  $t$ ) of a general form that does not contradict the unitarity of the  $S$ -matrix in the crossed channel:

$$A(s, t) = is^{\alpha(t)}F(\ln(s), t), \quad (42)$$

where  $F$  is a slow function of  $\ln(s)$  rapidly decreasing with an increase of  $-t$ . The positive value of  $d\alpha(t)/dt$  at  $t = 0$ , which follows from the positive value of the partial waves ( $\text{Im}f_l(s) \geq 0$ ) and properties of the Legendre polynomials [15], leads to a decrease in the average  $-t$  for elastic scattering with an increase in  $s$ .

Thus, the self-consistency of the theory requires that the radius of the hadron–hadron interaction should increase with energy.

V. Gribov [26] suggested that amplitudes of high energy processes are dominated by the special Regge pole trajectory exchange with the vacuum

quantum numbers in the crossed channel and calculated elastic and total cross sections. In parallel, G. Chew and S. Frautschi [22] also drew attention to the hypothetical Regge pole with  $\alpha(0) = 1$  and the vacuum quantum numbers that would be responsible for the forward scattering processes. This hypothesis reproduces the Pomernanchuk theorem and leads to an increase of the radius of the interaction with energy [14, 15, 26, 27]:

$$\begin{aligned}
 A(hT) &= g_{h\mathcal{P}h}(t)g_{T\mathcal{P}T}(t) \frac{\left(\frac{s}{s_0}\right)^{\alpha_{\mathcal{P}}(t)} + \left(\frac{u}{u_0}\right)^{\alpha_{\mathcal{P}}(t)}}{\sin(\pi\alpha_{\mathcal{P}}(t))} \\
 &= \frac{g_{h\mathcal{P}h}(t)g_{T\mathcal{P}T}(t) \left(\frac{s}{s_0}\right)^{\alpha_{\mathcal{P}}(t)} \exp(i\pi\alpha_{\mathcal{P}}(t)/2)}{\sin(\pi\alpha_{\mathcal{P}}(t)/2)} \quad , \quad (43)
 \end{aligned}$$

where  $g_{h\mathcal{P}h}(t)$  and  $g_{T\mathcal{P}T}(t)$  are the residues of the Pomeron pole. The signature factor follows from the symmetry of the amplitude due to the Pomeron exchange under the  $s \leftrightarrow u$  transformation as explained in the previous section.

#### 4.1.1 Experimental evidence for the Pomeron trajectory

The Pomeron trajectory is usually parametrized as a trajectory linear in  $t$ :

$$\alpha_{\mathcal{P}}(t) = \alpha_{\mathcal{P}}^0 + \alpha'_{\mathcal{P}}t. \quad (44)$$

The observed dependence of the total cross section of  $pp$  collisions on energy, which ranges from the fixed target energies to the highest energies currently measured at the LHC ( $\sqrt{s}=7$  TeV), is well described by the Pomeron intercept [28]:

$$\alpha_{\mathcal{P}}^0 \approx 1.08 - 1.1. \quad (45)$$

The generally accepted value of the slope of the Pomeron trajectory is

$$\alpha'_{\mathcal{P}} \approx 0.25 \text{ GeV}^{-2}. \quad (46)$$

The hypothesis of the dominance of the Pomeron exchange in high energy processes has found a number of experimental confirmations. Let us briefly outline basic discoveries.

(i) The same Pomeron intercept describes the energy dependence of the total and elastic cross sections of  $pp$  collisions and of the total cross section

of exclusive photoproduction of  $\rho$  mesons off the proton target measured at HERA [28]. The cross section of exclusive photoproduction of  $J/\psi$  mesons increases with energy more rapidly, see a recent summary in [29] (for the explanation, see the following subsections).

(ii) The shrinking of the diffractive peak with an increase of the collision energy has been predicted in [22, 26] and observed in  $pp$  and  $p\bar{p}$  collisions (see the summary of the data in [31]). The data for  $\sqrt{s} \leq 1.8$  TeV are consistent with the Pomeron trajectory being linear for  $-t \leq 0.5$  GeV<sup>2</sup>.

(iii) The first LHC data [31] report the  $t$ -slope corresponding to a faster rate of the shrinkage: for  $\sqrt{s}$  between  $\sqrt{s} = 2$  TeV and  $\sqrt{s} = 7$  TeV,  $\alpha'_{\mathcal{P}}(-t < 0.15 \text{ GeV}^2) \sim 0.55 \text{ GeV}^{-2}$ ; this value significantly increases with energy for larger  $-t$ . The interference between the single and multi-Pomeron exchanges produces a qualitatively similar behavior which we illustrate below. At small  $t$ , the amplitude for the single Pomeron exchange is conveniently parametrized as:  $\text{Im}A_1 = c_1 s^{\alpha_{\mathcal{P}}(t)-1} \exp(Bt/2)$ . Taking into account interference with the double Pomeron exchange, we obtain for the square of the ratio of the full amplitude to the single Pomeron exchange amplitude:  $|\text{Im}A/\text{Im}A_1|^2 \approx 1 - 2(c_2/c_1)s^{2\alpha_{\mathcal{P}}(t/4)-\alpha_{\mathcal{P}}(t)-1} \exp(-Bt/4)$ , where  $c_i$  are positive and  $c_2/c_1$  can be evaluated in the color fluctuation model. This formula produces the minimum which moves to smaller  $t$  with an increase of energies. This phenomenon has been discussed in the eikonal models, see, e.g., [32]; the problems of this approximation will be discussed in section 6.

(iv) The global analysis of the world data on exclusive  $\rho$ -meson photoproduction [30] gives  $\alpha'_{\mathcal{P}} = 0.126 \pm 0.013(\text{stat.}) \pm 0.012(\text{syst.}) \text{ GeV}^{-2}$  indicating non-universality of the  $t$  dependence of the effective Pomeron trajectory, see Fig. 2. The non-universality can also be seen from the comparison of the  $t$  dependence of  $\alpha_{\mathcal{P}}(t)$  with the linear Pomeron trajectory that describes the  $pp$  data for the same energy interval. However the data do not exclude a possibility that  $\alpha'_{\mathcal{P}}$  for the  $\rho$  case is the same as for the  $pp$  case for  $-t \leq 0.15$  GeV<sup>2</sup>. Note here that selection of small  $t$  enhances the contribution of peripheral collisions and hence suppresses the effects of multi-Pomeron exchanges and of blackening of the interaction at small impact parameters discussed in the next subsections. The data also indicate that  $\alpha_{\mathcal{P}} \geq 1$  for the entire studied  $t$ -range ( $-t \leq 1 \text{ GeV}^2$ ). In the case of elastic photoproduction of  $J/\psi$ ,  $\alpha_{\mathcal{P}} \approx 1.2$  for forward scattering and  $\alpha_{\mathcal{P}} \approx 1$  for  $-t \approx m_{J/\psi}^2$ . Such a behavior is natural for the pQCD regime where double logarithmic terms are relevant for the interrelation between the  $t$  and  $s$  dependences [33].

(v) It is well known from the analysis of the ladder diagrams relevant

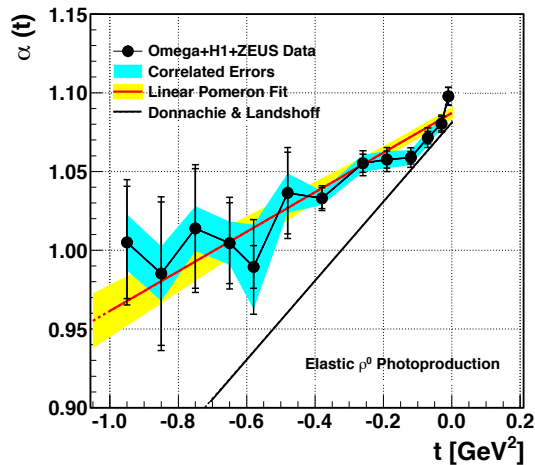


Figure 2: The data on the  $t$  dependence of the Pomeron trajectory as extracted from  $\rho$ -meson photoproduction with a linear fit to the data and the Donnachie–Landshoff parametrization of the  $pp$  data.

for the total DIS cross section [34] that  $\alpha'_{\mathcal{P}}$  decreases with the virtuality of the external probe due to the suppression of the Gribov diffusion in the impact parameter space. The observed value of  $\alpha'_{\mathcal{P}}$  for  $J/\psi$  photoproduction is definitely much smaller than that for  $pp$  scattering, see Eq. 104. However, the errors in the  $J/\psi$  case (see Eq. 104) do not allow one to establish whether  $\alpha'_{\mathcal{P}}$  extracted from the global analysis of the data for the  $J/\psi$  case is smaller than for the  $\rho$  case.

(vi) One of important confirmations of the dominance of the Pomeron exchange is the observation of the triple Pomeron diffraction [35, 36] at FNAL [37] and at the LHC [38], see the discussion in the next subsection.

The dominance of the Pomeron exchange in the total cross section allows for a relationship between the cross sections of diffractive and inelastic processes [39]. Thus, the total cross section of diffraction is unambiguously calculable in terms of the cross section of inelastic processes, i.e., diffraction in high energy processes is a shadow of inelastic processes.

## 4.2 Pomeron calculus

In this section we will discuss the physics of interacting Pomerons. The ideas and methods discussed in this section are now widely used in the evaluation of amplitudes of high energy processes, for a detailed discussion of the subject and proper references, see [17].

A single Pomeron trajectory generates multi-Pomeron branch points and related cuts in the angular momentum plane. This result follows from unitarity of the  $S$ -matrix for partial amplitudes continued into the angular momentum plane in the crossed  $t$ -channel [12, 40]. An exchange of  $n$  Pomerons leads to a branch point in the angular momentum plane located at [41, 12, 40]:

$$j(t)\alpha_{\mathcal{P}}(t/n^2) - n + 1 \approx n[\alpha_{\mathcal{P}}(0) - 1] + (\alpha'_{\mathcal{P}}/n)t. \quad (47)$$

Realization of the Pomeron in the form of ladder diagrams helped to develop the diagram technique [42], which allows one to calculate the contribution of any number of Pomeron cuts to the cross section and, hence, helped to develop the Pomeron calculus.

The simplest diagrams of the Pomeron calculus, which include a single Pomeron exchange, a two-Pomeron exchange, and a triple Pomeron exchange, are shown in Fig. 3. The coupling of two Pomerons to a hadron is expressed through the diffractive  $a + b \rightarrow X + b$  cross section that includes both the elastic and inelastic contributions. For  $t$  away from zero, the latter is enhanced as compared to the elastic contribution since the  $t$  dependence of diffraction is weaker than that of the elastic scattering. This is because in quantum mechanics form factor of bound state decreases significantly more rapidly with an increase in  $-t$  than does the form factor describing sum of inelastic transitions.

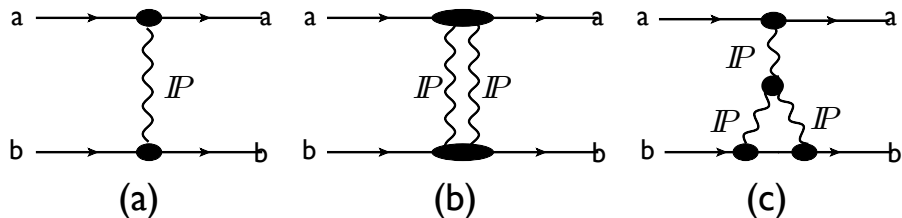


Figure 3: The single Pomeron exchange (a), the two-Pomeron exchange (b) and the triple Pomeron (c) diagrams.



If the intercept of the Pomeron were equal to unity ( $\alpha_P(0) = 1$ ), all branch points would be located at  $j = 1$  for  $t = 0$ . In this case, the calculation of the energy dependence of amplitudes of high energy processes leads to the scaling behavior of the Green's functions in the angular momentum plane in the vacuum channel. This technique developed in [43] helped to build the theory of second-order phase transitions and to analyze long-range fluctuations near the critical point.

There exists a variety of experimental evidences for the important role of multi-Pomeron interactions:

- (i) The triple Pomeron diffraction gives the pattern of how multi-Pomeron interactions arise, see the discussion in subsection 4.4;
- (ii) The shift to smaller  $-t$  of the position of the minimum of the elastic cross section with increase of energy indicates that the increase of the role of the multi-Pomeron exchanges with increase of  $s$  and  $t$ .
- (iii) The phenomenon of nuclear shadowing in hadron–nucleus collisions, where the incident hadron interacts with several nucleons of the nucleus, arises mostly due to multi-Pomeron exchanges.

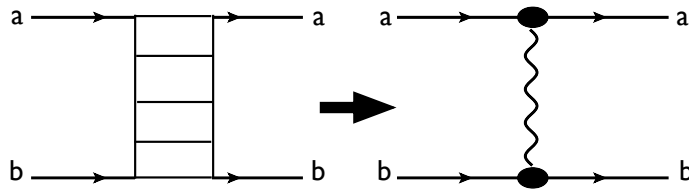


Figure 4: Ladder diagrams building the Pomeron exchange.

### 4.3 Gribov diffusion in the impact parameter space within the Pomeron ladder

The dynamical interpretation of the Pomeron exchange in the multiperipheral model or, equivalently, in the parton model, allows us to visualize the Pomeron in the phase space and to evaluate diffusion to large impact parameters. The Pomeron is modeled as the parton ladder (Fig. 4) where transverse momenta of produced partons are independent of energy,  $\langle k_t^2 \rangle = k_0^2$  [44, 45]. Experimental analyses of the transverse momenta distributions of produced pions and kaons show that  $\sqrt{k_0^2} \approx 0.3 - 0.4$  GeV/c. However, the majority of

observed mesons originate from decays of heavier hadrons (direct hadrons) which have significantly larger average transverse momenta  $\sqrt{k_0^2} \sim 0.5 - 0.6$  GeV/c already at moderate  $\sqrt{s} = 10 - 20$  GeV. The distances in rapidity  $\Delta y$  between partons adjacent in the ladder are independent of the collision energy. (The data on inelastic hadron production in high energy scattering find significant rapidity correlations between hadrons only for  $\Delta y \leq 1$ .) In a naive picture of the Pomeron described by a single ladder, each decay corresponds to a step of a random walk in the  $b$  space of the length  $\propto 1/k_0$  and the number of steps  $\propto \ln(s/\mu^2)/\Delta y$ . This leads to an increase of  $b^2$  with energy,  $b^2 \propto \ln(s/\mu^2)$ , and hence to finite  $\alpha'$  [44].

Diffusion to large impact parameters manifests itself directly in elastic hadron-hadron collisions. In the impact parameter space, the imaginary part of the partial amplitude due to the Pomeron exchange has the following form:

$$\text{Im}f(s, b^2) = \int \frac{d^2\vec{q}_t}{(2\pi)^2} \exp(i\vec{q}_t \cdot \vec{b}) \frac{A(s, q_t^2)}{2s} = \frac{cs^{\alpha_P(0)-1} \exp(-b^2/2B)}{B}, \quad (48)$$

where  $B = B_0 + 2\alpha'_P \ln(s/s_0)$  is the  $t$ -slope of the elastic cross section. We parametrize the product of the residues as  $c \exp(B_0 t/2)$  to take into account that Pomeron dynamics is dominated by peripheral, that is, small  $t$  processes.

It follows from Eq. 48 that the impact parameters essential for elastic  $pp$  collisions increase with energy as:

$$\langle b^2 \rangle_{\text{el}} \approx B_0 + 2\alpha'_P \ln(s/s_0). \quad (49)$$

In the case of the total cross section,

$$\langle b^2 \rangle_{\text{tot}} = 2 \langle b^2 \rangle_{\text{el}}. \quad (50)$$

Thus the assumption of the dominance of a single Pomeron exchange implies the dominance of peripheral collisions in hadron-hadron interactions at ultra high energies.

If spin-flip effects are neglected, the amplitude  $A(s, t)$  can be extracted from the differential cross section within the forward peak:

$$d\sigma_{\text{el}}/dt = \frac{1}{16\pi} |A(s, t)/s|^2. \quad (51)$$

In elastic  $pp$  collisions, spin-flip effects are small for  $-t \leq 1$  GeV<sup>2</sup> [46]. There exists an insignificant correction due to the possible ambiguity in the sign

of the amplitude beyond the cross section minimum, which for  $\sqrt{s} = 7$  TeV occurs at  $-t \approx 0.5$  GeV<sup>2</sup>. Thus the impact parameter distribution can be measured using the elastic cross section data.

The parton ladder model of the Pomeron allows us to evaluate properties of multi-Pomeron exchanges and Pomeron loops. To explain the role of multi-Pomeron exchanges, let us consider a simple model where the product of the Pomeron residues is parametrized as above by the factor of  $g_{h_1 \mathbb{P} h_1} g_{h_2 \mathbb{P} h_2} \exp B/2t$ . In this case the impact parameters corresponding to an exchange of  $n$  Pomerons rapidly decrease with  $n$ :

$$\langle b_n^2 \rangle \approx \langle b_{\mathbb{P}}^2 \rangle / n, \quad (52)$$

where  $\langle b_{\mathbb{P}}^2 \rangle = B$  are the impact parameters characteristic for the single Pomeron exchange;  $B$  is the slope of  $t$  dependence of the elastic cross section. (The inclusion of inelastic intermediate states for multi-Pomeron exchanges would result in a slower  $t$  dependence and, hence, in the further reduction of the average  $b^2$  for multi-Pomeron exchanges.)

The relative contribution of the multi-Pomeron exchanges as well as the effects of the Pomeron self-interactions grow with an increase of energy. As a result, the amplitude of the elastic  $pp$  collision becomes completely absorptive,  $\text{Im}f(b, s) \approx 1$  for small impact parameters, see the discussion in the next subsection. The blackness of the interaction at small impact parameters somewhat suppresses diffusion in the impact parameter space because the trajectories entering the absorption region disappear from Gribov diffusion.

Another effect leading to the suppression of Gribov diffusion is an increase with collision energy of the probability of hard processes with the corresponding tendency of the disappearance of significant differences between soft and hard QCD processes. It is rather difficult to observe this phenomenon directly since the majority of observed pions results from the decays of heavier resonances (section 4.3) which have average transverse momenta as high as 0.6 GeV/c already at fixed target energies.

#### 4.4 Observation of multi-Pomeron interactions: soft diffraction in the triple Pomeron limit

Probability of the processes with a large gap in rapidity can be evaluated using the Pomeron exchange. The Pomeron calculus predicts diffraction of an incident hadron into hadronic states whose invariant masses  $M_X$  are large

and the rapidity gap is large and increasing with energy,

$$h + T \rightarrow M_X + \text{rapidity gap} + T', \quad (53)$$

in the kinematics where  $M_X^2/s = x_{\mathcal{P}}$  is small and constant and  $s \rightarrow \infty$ . Here  $1 - x_{\mathcal{P}}$  is the fraction of the target momentum carried by the final state hadron  $T'$ . Since  $M_X$  is large and increases with  $s$ , the sum over diffractively produced states can be substituted by the Pomeron exchange for  $x_{\mathcal{P}} \ll 1$ . Thus the process of diffraction of an incident hadron into a large mass state probes the triple Pomeron vertex (the process corresponding to the diagram in Fig. 3c).

The observation of this process at FNAL [37] and the LHC [38] is a direct demonstration of how the Pomeron branch points arise and of their important role in high energy processes.

The consideration of the diagram *c* in Fig. 3 allows one to predict the dependence of the cross section on  $x_{\mathcal{P}}$  [35, 36]:

$$\begin{aligned} d\sigma(h + T \rightarrow "M_X" + \text{rapidity gap} + T')/dx_{\mathcal{P}}d^2q_t = & \quad (54) \\ s^{\alpha_{\mathcal{P}}(0)-1} g_{h\mathcal{P}h}(t=0) g_{T\mathcal{P}T'}^2(q_t^2) (1/x_{\mathcal{P}})^{2\alpha_{\mathcal{P}}(t)-1} x_{\mathcal{P}}^{\alpha_{\mathcal{P}}(0)-1} = & \\ s^{\alpha_{\mathcal{P}}(0)-1} g_{h\mathcal{P}h}(t=0) g_{T\mathcal{P}T'}^2(q_t^2) (1/x_{\mathcal{P}})^{\alpha_{\mathcal{P}}(0)-2\alpha'_{\mathcal{P}}q_t^2}, & \end{aligned}$$

where  $q_t$  is the transverse momentum transferred to the target. A distinctive feature of this formula is the singularity of the cross section at  $q_t = 0$  and  $x_{\mathcal{P}} \rightarrow 0$ , if the triple Pomeron vertex  $g_{3\mathcal{P}}(q_t = 0)$  is different from zero. If  $\alpha_{\mathcal{P}}(0) > 1$ , this singularity will be present at non-zero  $t$  as well. This singularity lies in the unphysical region since  $x_{\mathcal{P}} = 0$  requires infinite energies. With an increase of  $s$ , multi-Pomeron exchanges and Pomeron loops, which were effectively forbidden at lower energies by energy-momentum conservation, become progressively important.

Inelastic diffraction can occur only at large impact parameters since inelastic processes fill the rapidity gap at small impact parameters, where the interaction is practically completely absorptive. The Pomeron calculus takes this effect into account by including multi-Pomeron exchanges that strongly screen the triple Pomeron contribution, especially at small impact parameters. The overall effects are the reduction in the large-mass diffraction, a faster decrease in the cross section with  $q_t^2$ , and a reduction of  $\alpha_{\mathcal{P}}^{\text{eff}}(t \sim 0)$ . Screening of the triple Pomeron vertex was evaluated in the generalized eikonal approximation in [47] and was found to be very large. The behavior of inelastic diffraction in  $pp$  collisions that we described above has been

observed at FNAL [37]. Most of the FNAL data [37] correspond to relatively large  $x_{\mathcal{P}} > 0.01$  so that the contributions of secondary trajectories play an important role. The recent LHC data [38] observed similar regularities but at smaller  $x_{\mathcal{P}}$ , where the contribution of secondary trajectories can be neglected, while the screening effects may play a role;  $\alpha_{\mathcal{P}}^{\text{eff}} \approx 1.05$  was reported [38].

## 4.5 Blackening of hadron–hadron interactions at central impact parameters

Probability conservation, i.e., unitarity of the  $S$  matrix in the  $s$ -channel, restricts the high energy behavior of the total cross sections of hadronic collisions and cross sections of diffractive processes:

$$\text{Im } f(b, s) = \frac{1}{2} |f(b, s)|^2 + \text{positive terms} . \quad (55)$$

High energy processes are predominantly inelastic so that the partial waves are predominantly imaginary. Indeed, it follows from Eq. 55 together with the expression for the cross section of inelastic processes [48] that:

$$\sigma_{\text{inel}}(s, b) = 1 - |S_l - 1|^2 , \quad (56)$$

where  $S_l = 1 + if_l$  is the matrix element of the  $S$ -matrix corresponding to the orbital momentum  $l$ . If  $\text{Im } f(b, s)$  exceeds unity,  $\sigma_{\text{inel}}(s, b)$  would start decreasing with an increase of  $\text{Im } f(b, s)$  in contradiction with the dominance of inelastic processes. As a result, one concludes that at high energies the partial waves for elastic collisions cannot exceed unity:

$$\text{Im } f(b, s) \leq 1 . \quad (57)$$

The upper boundary for the total cross section follows from the  $S$ -matrix theory [7]. Indeed, if in the kinematical region of  $t$  restricted by the singularities of the amplitude in  $t$  plane the scattering amplitude increases with energy not faster than a polynomial, i.e., if  $\text{Im } A(s, t) \leq s^N$ , then

$$\sigma_{\text{tot}} \leq c \ln^2(s/s_0) . \quad (58)$$

The formal derivation [49] uses analytic properties of the amplitude in the  $t$ -plane and unitarity of the  $S$ -matrix to derive the polynomial boundary on

the amplitude that we mentioned above. This derivation also allows one to evaluate the coefficient  $c$  in Eq. 58 whose value turns out to be unrealistically large, being significantly larger than that arising from fits to the  $pp$  data.

As we explain above, the amplitude  $A(s, t)$  can be unambiguously extracted from the data on elastic  $pp$  collisions using Eq. 51. In the kinematics achieved at FNAL for  $pp$  scattering,  $\sigma_{\text{tot}}(pp) \approx 16\pi B$ . This means that for the  $pp$  interaction at the zero impact parameters, the partial amplitude is close to unity. If we define (for the illustration purposes) proximity to the black regime as a condition that probability of the inelastic interaction is  $\geq 0.75$  (see Eq. 56), the interaction will be close to being black for  $b \leq 1.0$  fm at  $\sqrt{s} = 7$  TeV and for  $\sim 15\%$  smaller values of  $b$  at  $\sqrt{s} = 2$  TeV. For larger  $b$ , which dominate in the inelastic cross section (the median  $b \sim 1.4$  fm at  $\sqrt{s} = 7$  TeV), the interaction is grey and rather far from the black regime.

It is well known from textbooks that the assumption that the interaction is black at all impact parameters leads to the following two predictions:

$$\sigma(hT)_{\text{el}}/\sigma(hT)_{\text{tot}} = \frac{1}{2} \quad (59)$$

and

$$d\sigma/dt(pp \rightarrow \text{diffractive state} + \text{rap. gap} + p)_{t=0} = 0. \quad (60)$$

The second property of the black disc regime (BDR) follows from orthogonality of the wave functions of the eigenstates of the Hamiltonian corresponding to different eigenvalues.

Eq. 59 is in the evident disagreement with the data as the  $\sigma_{\text{el}}/\sigma_{\text{tot}}$  ratio at the LHC, while slowly increasing with energy, still reaches only the value of about 25%. Also, at the LHC the ratio of inelastic and elastic diffraction is close to unity in the apparent contradiction with Eq. 60. Taken together, the discussed features of the data point out that, effectively, the  $pp$  scattering at FNAL and the LHC has a small black spot at small  $b$  surrounded by a large grey area. The grey part mostly represents the contribution of peripheral collisions to the total cross section and it is dominated by exchanges of the Pomeron and Pomeron cuts.

## 5 Space–time evolution of high energy processes

### 5.1 Introduction

The phenomenon of the linear increase of longitudinal distances with an increase of the collision energy was first understood in QED for the propagation of charged particles through the medium and led to the so-called Landau–Pomeranchuk–Migdal effect [50]. In QCD, the linear increase of longitudinal distances with the collision energy [51] is a fundamental property of high energy processes. This and following sections discuss new coherent phenomena that follow from taking into account the space–time evolution of high energy processes in QCD. Note that the concept of the space–time evolution of high energy processes [52] is beyond the framework of the  $S$ -matrix approach. The aim of this section is to explain some properties of the space–time evolution of the scattering processes and their implications.

### 5.2 Linear increase of longitudinal distances in high energy processes with energy

It follows from the application of the energy–time uncertainty principle to scattering processes in QCD that when the energy of the projectile in the target rest frame,  $E$ , is large enough, the quark–gluon configurations satisfying the condition:

$$z \approx (1/(\Delta E)) \approx 2E/(M^2 - m_h^2) \gg R_T \quad (61)$$

are formed before the target and these configurations are frozen before the collision. In Eq. 61,  $(M^2 - m_{hadron}^2) = \sum_i (m_q^2 + k_{i,i}^2)/z_i - m_{hadron}^2$  and  $z_i$  is the fraction of the incident particle momentum carried by the constituent  $i$ . Thus, the space–time evolution of the scattering processes differs from that in non-relativistic physics. Eq. 61 directly follows from the Lorentz transformation applied to projectiles with an energy-independent number of constituents. One can easily check the validity of the above estimate of longitudinal distances by analyzing the dominant ladder diagrams using popular approaches to high energy processes.

Here we will present reasonings applicable also in the non-perturbative QCD regime. Let us consider the virtual photon–target scattering in the deep inelastic (Bjorken) limit:  $-q^2 \rightarrow \infty$ ,  $-q^2/2(q \cdot p_T) = \text{const}$ , where  $q$

and  $p_T$  are the four-momenta of the photon and the target, respectively. It follows from the optical theorem that the total  $\gamma^*$ -target cross section has the following form:

$$\sigma = \frac{1}{s} \text{Im} A(\gamma^* + T \rightarrow \gamma^* + T) = \frac{1}{s} \int \exp(iq \cdot y) \langle T | [J_\mu(y), J_\mu(0)] | T \rangle d^4y. \quad (62)$$

As a consequence of causality, only the  $y^2 = t^2 - z^2 - y_t^2 \geq 0$  region contributes to Eq. 62. At large energies,  $q_0 = \sqrt{q_z^2 - Q^2} \approx q_z - Q^2/2q_z$  and, thus,  $i(q \cdot y) \approx i(q_0(t - z) - zQ^2/2q_0)$ . Since the  $Q^2$  dependence is contained only in the second term and the cross section decreases with an increase of  $Q^2$ , the direct analysis of the representation of the cross section in the form of Eq. 62 shows [51] that essential distances in the integral are  $t \approx z$  and

$$z \approx 2q_0/Q^2. \quad (63)$$

### 5.3 Cancellation of the contribution of planar/Glauber-approximation diagrams

It has been understood long ago that the Glauber (eikonal) approximation—being a very popular method of modeling of high energy processes in nuclear and particle physics—is actually inapplicable beyond the non-relativistic domain. The dominance of large longitudinal distances changes qualitatively the pattern of multiple interactions.

In the non-relativistic quantum mechanics, the eikonal approximation follows from the Schrodinger equation when the kinetic energy of the incident particle significantly exceeds the potential of the interaction [48]. In the Glauber approximation, high energy interactions of the projectile with a target occur via consecutive rescatterings of the projectile off the constituents of the target. The projectile is on its mass shell between the interactions—one takes the residue in the propagator of the projectile (Fig. 5a). However, the Glauber approximation contradicts the QCD-based space-time evolution of high energy processes dominated by particle production. Indeed, as the essential distances become significantly larger than the distances (time intervals) between consequent rescatterings [51], there is no time for a frozen configuration in the projectile to recombine into the projectile during the time of the order of  $R_T$  since it is much shorter than the lifetime of the configuration (Eq. 61).



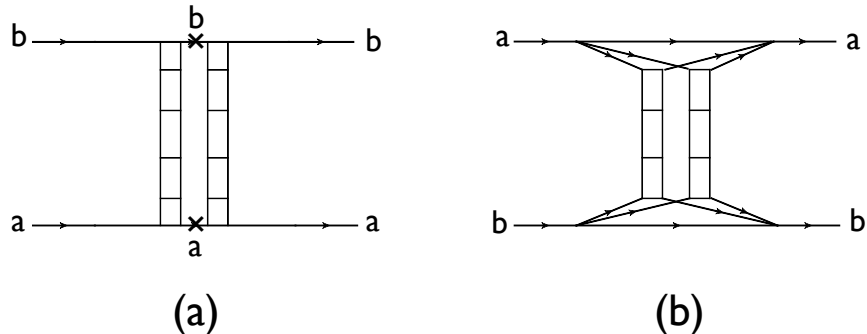


Figure 5: (a) The planar diagram for double scattering. (b) A non-planar diagram for double scattering.

There are two independent theoretical proofs that the contribution of planar diagrams to the double Pomeron scattering amplitude is actually zero. It was found that in the case of high energy scattering in a quantum field theory, the contribution of the planar diagrams with intermediate states corresponding to the projectile on its mass shell drops with the incident energy as  $1/s$ . Indeed, the integral over the square of the mass of hadrons produced in the  $\mathbb{P}$ -hadron collision,  $M^2$ , is zero in the case when the Feynman diagrams have only  $s$  or  $u$  cuts because the contour of integration can be moved in the direction where there are no singularities in  $M^2$  [41, 42]. The integral over the large circle is zero as a consequence of a decrease of the amplitude with  $M^2$ . The eikonal diagram (Fig. 5a) belongs to the class of Feynman diagrams where the cancellation occurs. Crossed (non-planar) diagrams (Fig. 5b), which have cuts both in  $s$  and  $u$ , give a non-zero contribution.

Taking in account energy-momentum conservation leads to the same conclusion [53]. Indeed, the eikonal diagrams correspond to an inelastic intermediate state described by the Pomeron exchange at the double energy  $2s$ . On the contrary, in the crossed diagram *the energy is divided between constituents before the collision*. If one parton carries the fraction  $z$  of the incident hadron momentum and another parton carries the fraction  $z' \leq 1 - z$ , the total energy of the produced hadronic state is  $sz + sz' \leq s$ . Both arguments can be easily generalized to the case when the wave function of the initial hadron contains many constituents.

Using the technique of the Pomeron calculus, V. Gribov showed that in a

quantum field theory, the contribution of the non-planar diagrams relevant for the multiple Pomeron exchanges to the total cross section can be rewritten as a sum of the eikonal term and the inelastic diffraction contribution. The resulting Gribov–Glauber model [54] is in agreement with the data on nuclear shadowing in hadron–nucleus interactions [55]. We will explain in section 6.4 how taking into account color fluctuations allows one to evaluate the relative contributions of multiple scatterings in the Gribov–Glauber model.

## 6 Fluctuations of color in diffractive phenomena

### 6.1 Introduction

QCD predicts new types of diffractive phenomena as compared to the  $S$ -matrix approach since the wave function of an energetic incident hadron is formed long before the target and the transitions between different configurations in the wave function occur at distances comparable with the characteristic longitudinal distance called the coherence length. Therefore, the cross section is calculable in terms of the instant quark–gluon configurations in the projectile (see the discussion in the previous section). In the exclusive processes, where the incident hadron is squeezed in the transverse direction by the choice of the specific final state, the spatially small wave packet of quarks and gluons weakly interacts with a target in a rather large interval of collision energies. This phenomenon is calculable for hard diffractive processes in the form of the special QCD factorization theorem [34, 56] and has been observed in a variety of experiments (see section 7.7 and the review and references in [57]). Thus QCD predicts fluctuations in the strength of the interaction since the interaction differs for different configurations of constituents in the wave function of the incident hadron. This is an intuitive justification of the necessity to use the concept of the distribution over cross sections instead of the average cross section.

### 6.2 Suppression of the strong interaction due to screening of color

At large energies the wave function of the incident hadron is formed before the target and is frozen, if  $(2E/\Delta M^2) \gg R_T$ . Different configurations of

constituents in the wave function of the incident hadron interact with the target at different strengths. This is an important property of QCD where the interaction is proportional to the area occupied by color since the color charge of a hadron is zero. For illustration purposes we begin with quark models of hadrons and then derive formulas in QCD.

A popular model was suggested by Low and Nussinov [58, 59] in which the total hadron–hadron cross section is described by the exchange of two gluons. Low further argued that the cross section is proportional to the region occupied by color in the hadrons:

$$\sigma(hT) = cr_t^2, \quad (64)$$

where  $r_t$  is the transverse radius of the smaller hadron. The derivation involves taking into account the gauge invariance, the zero color charge of hadrons as well as an implicit assumption that the momenta of constituents within the hadrons are significantly larger than the transverse momenta of the exchanged gluons. Eq. 64 was elaborated on in the constituent quark model with a two-gluon exchange between  $h$  and  $T$  [60]. Eq. 64 can be questioned since in the model, the average size of configurations involved in the scattering is comparable to the scale of non-perturbative QCD phenomena and the restriction by a two-gluon exchange cannot be justified.

Eq. 64 can be reformulated to include the full QCD. If the incident meson is in a quark-gluon configuration whose transverse size is significantly smaller than the scale of non-perturbative QCD phenomena,  $r_t^2 \Lambda_{QCD}^2 \ll 1$ , the application of the technology of the QCD factorization theorem [56] and the QCD evolution equation for parton densities allows one to calculate the cross section of the hadron interaction with a target  $T$ . The derived expression [61, 62, 63] also contains the factor of  $r_t^2$  as in Eq. 64 which represents the coordinate space equivalent of approximate Bjorken scaling for DIS processes. However, in addition, the final expression contains the factor  $xG_T$ —the gluon distribution in the target  $T$  absent in Eq. 64:

$$\begin{aligned} & \sigma_{hT}(r_t \rightarrow 0) \Big|_{4r_t^2 s/m_N \gg R_T} \\ &= \psi_h^2(r_t = 0, r_z = 0) \frac{F^2 \pi^2}{4} r_t^2 \alpha_s(Q^2) xG_T(x, Q^2 = \frac{1}{4r_t^2}). \end{aligned} \quad (65)$$

Here  $F^2$  is the Casimir operator for the quark (gluon) dipole;  $r_t$  is the transverse distance between the quark and the antiquark;  $\psi_h(r_t)$  is the small transverse size component of the incident hadron wave function;  $x \sim 1/(4sr_t^2)$ .

Eq. 65 can be obtained also from the formulae derived in [64] in the leading  $\alpha_s \ln(x_0/x)$  approximation. In the case of nucleon one needs to take into account that the square of nucleon wave function at small  $r_{it}$  is proportional to  $r_{it}^2$  and to make the substitution

$$r_t^2 \rightarrow (r_{t1} - (r_{t2} + r_{t3})/2)^2 + (r_{t2} - (r_{t1} + r_{t3})/2)^2 + (r_{t3} - (r_{t1} + r_{t2})/2)^2. \quad (66)$$

In this case, the three quarks act as a symmetrized superposition of three dipoles stretched between one quark and the transverse center of mass of the other two quarks.

### 6.3 Perturbative Pomeron

The asymptotic behavior of the amplitudes of high energy processes in the vacuum channel in a quantum field theory containing vector particles was first investigated in QED. In [65] the sum of the leading  $\alpha_{em}^2 \ln(s/s_0)$  terms in the cross section of the photon–photon scattering was calculated. (Note that in QED, in the lowest–order over coupling constant, this cross section is independent of energy.) This idea was applied to QCD in [66, 67] to study amplitudes of high energy processes in the kinematics where  $\ln(x_0/x) \gg \ln(Q^2/Q_0^2)$  by summing leading  $\alpha_s \ln(x_0/x)$  terms—the so-called perturbative Pomeron. A priori one can try to justify this approximation in the case of scattering of two small dipoles of the transverse size  $\propto 1/Q$  within the restricted kinematical domain of rapidities  $y \leq y_0(Q^2, x)$ , where the coupling to the colliding dipoles is perturbative. The kinematical boundary for the applicability of this approximation— $y_0(Q^2, x)$ —as well as for the decomposition over powers of  $1/Q^2$  arises due to diffusion in the space of transverse momenta to the non-perturbative domain [68].

In the leading log approximation, the cross section grows as:

$$\sigma_{\text{dipole-dipole}} \propto (1/x)^\beta, \quad (67)$$

where

$$\beta = \frac{N_c \alpha_s 4 \ln 2}{\pi}. \quad (68)$$

For  $Q^2 \sim 2 \text{ GeV}^2$ ,  $\alpha_s \sim 0.25$  leading to  $\beta \approx 0.7$ . Note that the actual formula derived in [66, 67] is significantly more complicated than Eq. 68, which is just a popular fit to this formula. The derived expression [66] corresponds to a cut in the angular momentum plain so that it involves a mathematical object

that is different from the Pomeron Regge trajectory discussed in section 4. It becomes a sum of the poles in the angular momentum plane in the large  $N_c$  approximation.

Assuming that the number of radiated gluons is sufficiently large, the diffusion equation was derived for the motion in the plane of  $\ln(p_t^2/p_{t0}^2)$ . It was observed that diffusion both to large and small  $p_t$  is present [66, 69]. Significant diffusion to small  $p_t$ , i.e., into the non-perturbative domain raises questions about the validity of pQCD approach because the answer depends on the treatment of the badly understood infrared region. The main difference between the perturbative Pomeron and the Pomeron trajectory discussed in section 4 is significant diffusion to large parton momenta (in addition to diffusion to small parton momenta). Such diffusion is absent in the non-perturbative Pomeron which is modeled by the non-perturbative ladder discussed in section 4.

The NLO correction to Eq. 68 was found to be so large [70, 71] that it dominates the LO expression for a wide range of  $\alpha_s$ , which leads to  $\beta \sim 0$ . This is primarily because the LO as well as NLO approximations ignore energy–momentum conservation. The poor convergence of the series for the total cross section in terms of powers of  $\ln(s/\mu^2)$  was first demonstrated in QED [72] by the direct calculation of the lowest order diagrams for the  $e^+e^-$  pair production in electron–electron scattering. For the contribution of the dominant two-photon mechanism, it was found that

$$\sigma = \alpha_{\text{em}}^4 c (1.04 \ln^3(s/\mu^2) - 6.59 \ln^2(s/\mu^2) - 11.8 \ln(s/\mu^2) + 104 + O(\mu^2/s)), \quad (69)$$

where  $\mu$  is the electron mass. It was explained in [72] that a fast growth of the coefficients in front of the powers of  $\ln(s/s_0)$  reflects the highly restricted phase space for obtaining logarithmic contributions.

The resummation models [73, 74] more smoothly match with the formulas of the DGLAP approximation where the conservation of the longitudinal component of the momentum is exact.

The same approach is often applied to scattering of a small dipole of the diameter  $d \approx 1/Q$  off the nucleon whose diameter is  $\approx 1/(2m_\pi)$ , which is relevant for such processes as inclusive DIS, exclusive production of vector mesons, etc. Although the energy behavior given by Eq. 67 obviously contradicts the data, resummation approaches can fit the data since they lead to the results close to those obtained in the DGLAP approximation. Up to now the resummation approaches have not been applied to the description

of hard diffractive processes.

One should note that the probability conservation in the form of Eq. 118 is also violated in the resummation models at sufficiently small  $x$  and small impact parameters (see the discussion in section 8).

## 6.4 Distributions over strengths of the interaction for hadron and photon projectiles

Before QCD was recognized as the theory of the strong interactions, in the framework of the parton model in which the strength of interactions is proportional to a number of wee partons in the projectile configuration, Pumplin and Miettinen suggested the description of high energy diffractive processes in terms of the probability distribution over cross sections,  $P_h(\sigma)$  [75]. It was understood later on that such a distribution originates from the dependence of the cross section on the instant transverse radius of the color distribution in the incident hadron.

Constructively,  $P_h(\sigma)$  is defined in terms of its moments,

$$\langle \sigma^k \rangle = \int P_h(\sigma) \sigma^k d\sigma, \quad (70)$$

with additional general QCD restrictions on the form of  $P_h(\sigma)$ . The case of  $k = 0$  corresponds to the normalization condition for  $P_h(\sigma)$ . By definition, the first moment of  $P_h(\sigma)$  ( $k = 1$ ) is the total cross section of  $hN$  scattering. The dispersion of the distribution over  $\sigma$  is given by the ratio of inelastic and elastic diffraction at  $t = 0$  [75]:

$$\frac{d\sigma(h + N \rightarrow h' + N)/dt|_{t=0}}{d\sigma(h + N \rightarrow h + N)|_{t=0}} = \frac{\langle \sigma^2 \rangle - \langle \sigma \rangle^2}{\langle \sigma \rangle^2} \equiv \omega_\sigma. \quad (71)$$

where the state  $h'$  differs from the state  $h$ .

The behavior of  $P_h(\sigma)$  at small  $\sigma$  follows from the kind of quark counting rules. Taking into account the number of valence quarks in a hadron  $h$  and using approximate Bjorken scaling in the form explained above ( $\sigma \propto r_t^2$ ), it was found that [61, 76]:

$$P_h(\sigma \rightarrow 0) \propto \sigma^{(n_q + n_{\bar{q}} + n_g - 2)}, \quad (72)$$

where  $n_i$  is the number of valence constituents in the incident hadron in the configuration participating in the scattering process<sup>1</sup>. The data on diffractive

---

<sup>1</sup>In the analysis of [75] it was assumed that  $P_N(\sigma)$  contains the term  $\propto \delta(\sigma)$ .

$p+^2H \rightarrow X+^2H$  scattering provides an additional constraint,  $\langle(\sigma - \langle\sigma\rangle)^3\rangle \approx 0$  at  $\sqrt{s_{NN}} = 30$  GeV [76]. The information on the first three moments of  $P_h(\sigma)$  and its behavior at  $\sigma \rightarrow 0$  allows one to reconstruct the form of  $P_h(\sigma)$  for the pion and nucleon projectiles (Fig. 6).

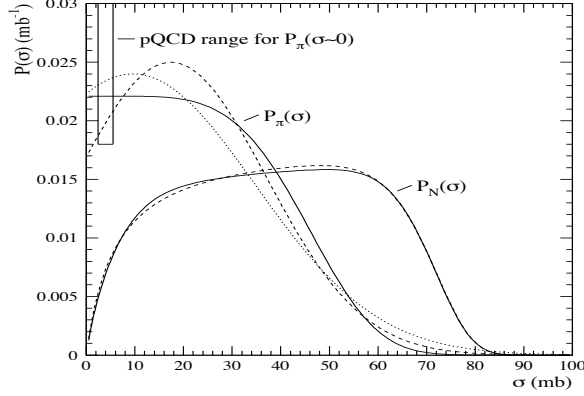


Figure 6: The distribution over  $\sigma$  for fixed target energies extracted in [76]. The set of curves reflects uncertainties in the extraction procedure. The rectangular area in the upper left corner is the pQCD evaluation of  $P_\pi(\sigma \rightarrow 0)$  [63].

At present, the distributions are reconstructed for the energies of incident hadrons in the range of a few hundred GeV in the target rest frame. With an increase of the energy, the edge of the distribution moves to the right diminishing probability of weakly interacting configurations. The dispersion of the distribution grows with  $\sqrt{s}$  up to  $\sqrt{s} = 50-100$  GeV, where  $\omega_\sigma \sim 0.3$  is reached, and it starts dropping for larger  $\sqrt{s}$ . Preliminary LHC data indicate that for  $pp$  scattering at  $\sqrt{s}=7$  TeV,  $\omega_\sigma \sim 0.2$ . Note that  $\omega_\sigma \sim 0.2 - 0.3$  corresponds to very large fluctuations of the strength of the interaction. For example, if one models  $P_N(\sigma)$  as a superposition of two scattering states,  $\sigma$ 's for these states would be  $\sigma_{\text{tot}}(1 \pm \sqrt{\omega_\sigma})$  corresponding to  $\sigma_1 \sim 55$  mb and  $\sigma_2 \sim 145$  mb at  $\sqrt{s} = 7$  TeV.

In the case of photon,

$$P_\gamma(\sigma \rightarrow 0) \propto 1/\sigma, \quad (73)$$

which follows from the presence of point-like  $q\bar{q}$  configurations in the photon the wave function.

The Gribov–Glauber model allows for a transparent interpretation in the formalism of cross section eigenstates of Good and Walker [77]. Indeed, different configurations are absorbed with the strength given by the Glauber model for a given  $\sigma$  and incoherently contribute to the total cross section [78].

The concept of  $P_h(\sigma)$  allows us to build a compact implementation of the Gribov–Glauber series for the total cross section of  $hA$  scattering:

$$\sigma_{\text{tot}}(hA) = \int d\sigma P_h(\sigma) \int d^2b 2[1 - e^{-\sigma T_A(b)/2}]. \quad (74)$$

It allows us also to calculate the total cross section of inelastic coherent diffraction off nuclei ( $hA \rightarrow h'A$ ) in a good agreement with the data [79, 80, 81]. It also allows us to model deviations from the Glauber model in inelastic proton (nucleus)–nucleus collisions [82]. Note here that deviations from the eikonal approximation for the interactions with  $j$  nucleons is given by the  $\langle \sigma^j \rangle / \langle \sigma \rangle^j$  ratio, which rapidly grows with  $j$ .

Knowledge of the first three moments of the distribution over  $\sigma$  is sufficient to describe many nuclear phenomena, in particular, the total and coherent inelastic diffraction cross sections. The evaluation of more complicated phenomena such as, the tail of the hadron multiplicity, at present is model-dependent since the behavior of  $P_h(\sigma)$  at large  $\sigma$  is far from being understood.

## 6.5 Diffraction in deep inelastic collisions as a pattern for the fluctuations of color

In this subsection we will consider diffraction in deep inelastic  $ep$  scattering:

$$\gamma^* + p \rightarrow X + \text{rapidity gap} + p \quad (75)$$

in the Bjorken limit.

The standard picture of DIS is that of the absorption of the virtual photon by a parton (quark or antiquark) that carries a fraction  $x$  of the light-cone momentum of the nucleon with radiation of gluons in the initial and final states. In such a picture, which was quite popular before the first measurements at HERA, the hard gluon radiation should fill the whole available rapidity interval (in addition, partons should be emitted to screen the delocalized color in the final state) and lead to the disappearance of diffractive



processes. However, such processes were observed with a significant probability even at very large  $Q^2$ .

We will focus our attention on the limit when  $M_X^2/Q^2 = \text{const}$ . In this limit, it is convenient to introduce the variable  $\beta$ :

$$\beta = \frac{Q^2}{Q^2 + M_X^2}. \quad (76)$$

The variable  $\beta$  is related to the fraction of the momentum lost by the nucleon,  $x_{\mathcal{P}}$ , as

$$\beta = x/x_{\mathcal{P}}. \quad (77)$$

It is convenient to introduce "conditional" or fracture structure functions for the processes where one hadron is fixed in the fragmentation region. For diffractive processes, one usually uses the notation  $F_p^{D(4)}(\beta, Q^2, x_{\mathcal{P}}, t)$  and one can also introduce quark and gluon diffractive parton distribution functions (PDFs) that depend on the same variables. Since hard processes occur locally in transverse momenta and rapidity, the increase in the resolution should not affect the properties of the nucleon fragmentation region. Hence one should expect that the diffractive PDFs should satisfy the same DGLAP evolution equations as usual PDFs.

Extensive data on various large-mass diffractive processes have been obtained at HERA (for the recent results, see [83]). The principal findings are the following:

- The leading twist approximation with the same diffractive PDFs consistently describes the  $Q^2$  evolution of the inclusive diffractive cross section and the diffractive cross sections of dijet ( $X = \text{jet}_1 + \text{jet}_2 + X'$ ) and heavy flavor production for fixed  $x_{\mathcal{P}}$ . Factorization was formally proven in [84].
- The data are also consistent with the Pomeron factorization:

$$f_j^{4D}(\beta, Q^2, x_{\mathcal{P}}, t) = r(x_{\mathcal{P}}, t) f_j(x, Q^2). \quad (78)$$

The  $x_{\mathcal{P}}$  dependence of  $r(x_{\mathcal{P}}, t)$  is given by the same expression as that for soft diffraction, which employs  $\alpha_{\mathcal{P}}(0) = 1.11$ , which is close to  $\alpha_{\mathcal{P}}(0)$  extracted from the analysis of soft diffractive processes, total  $pp$  cross sections, and exclusive light vector meson photoproduction (subsection 5.2). The observed value of the intercept is significantly smaller than  $\alpha_{\mathcal{P}}(0)$  for such hard exclusive diffractive processes as  $J/\psi$  photo(electro)production. It was also

found that gluons play a very important role in diffractive dynamic:

$$\frac{\int_0^1 d\beta \beta f_g(\beta, Q^2)}{\sum_{q_i, \bar{q}_i} \int_0^1 d\beta \beta f_{q_i}(\beta, Q^2)} \sim 4 \quad (79)$$

for  $Q^2 \sim$  a few  $\text{GeV}^2$ .

- The overall probability of diffraction in DIS

$$R(x, Q^2) = \sigma_{\text{diff}}(x, Q^2) / \sigma_{\text{DIS}}(x, Q^2), \quad (80)$$

is of the order of 10% and grows with a decrease of  $x$  for fixed  $Q^2$ .

As we mentioned above, hard processes cannot screen the quark (anti-quark) emitted by a highly virtual photon. Therefore, pQCD states should contain no rapidity gaps and, thus, diffraction should be part of the non-perturbative initial condition for the QCD evolution equation, which is far from trivial to implement in the infinite momentum frame. *The presence of the leading twist diffraction imposes constraints on sea quark and gluon nucleon PDFs at the starting point of the evolution—they should exhibit the small  $x$  behavior consistent with the soft Pomeron limit, i.e., they are allowed to grow only slowly with a decrease of  $x$ .*

The significant value of the cross section of diffraction can be understood in the formulation of the parton model in the target rest frame suggested by Bjorken in 1970 twenty years before diffraction in DIS was observed. At small  $x$  in this reference frame, the virtual photon transforms into  $q\bar{q}$  pairs well before the target (section 6). To satisfy Bjorken scaling, it is necessary to assume that only the  $q\bar{q}$  pairs with  $k_t \leq k_{t0}$  and the light-cone fractions satisfying the condition  $k_{t0}^2 / z(1-z) \sim Q^2$  should interact with the target at small  $x$  with a strength comparable to that of the pion–nucleon interaction, while the contribution of the pairs with  $k_t \gg k_{t0}$  should be strongly suppressed. The low  $k_t$  pairs are aligned along the photon direction—hence they are referred to as the aligned jet model (AJM) [85]. The  $1/Q^2$  behavior of this contribution is due to the small phase space allowed for these configurations. In the coordinate space this corresponds to production of a  $q\bar{q}$  pair at a distance  $2q_0/Q^2$  from the target and the expansion of the pair to the hadronic-scale size of  $1/k_{t0}$  by the time it reaches the target [86].

In QCD, the parton picture is modified by the following two effects. First, the emission of a large-size  $q\bar{q}$  pair without the associated gluon emission is suppressed by the Sudakov form factor. Inclusion of this emission

leads to the scaling violation, but it does not change the size of the quark–gluon configuration—the QCD AJM [87]. Second, while the interaction of  $q\bar{q}$  pairs with the large transverse momenta up to  $k_t \propto Q$  is suppressed by the  $1/Q^2$  factor due to color transparency, it also contains the factor  $\alpha_s(Q^2)xG_N(x, Q^2)$ . As a result, there is conspiracy between the hard and soft contributions—both of them are  $\propto 1/Q^2$ , with the hard contribution being numerically suppressed at moderate  $x \sim 10^{-2}$ , but gradually growing in importance with a decrease in  $x$  due to the corresponding increase in  $xG_N$ . The contribution of large masses  $\gg Q^2$ , i.e.,  $\beta \ll 1$  (the triple Pomeron processes) requires sufficiently small  $x$  to reveal itself. Otherwise, it is suppressed by energy–momentum conservation.

Thus, the probability of diffraction in the aligned jet model (DGLAP approximation) is comparable to that in hadron–nucleon scattering. At the same time, the contribution of small-size configurations to the cross section of diffraction (integrated over  $\beta$ ) is suppressed relatively to the inclusive cross section by the factor

$$\frac{\sigma_{\text{diff}}}{\sigma_{\text{tot}}|_{\text{hard}}} = c \frac{\alpha_s^2(Q^2)(xG_T(x, Q^2))^2/BQ^4}{\alpha_s xG_T(x, Q^2)/Q^2} \propto \alpha_s(Q^2)xG_T(x, Q^2)/BQ^2, \quad (81)$$

where  $B$  is the slope in the  $t$  dependence of the diffractive cross section. This ratio rapidly decreases with an increase in  $Q^2$  and increases (for fixed  $Q^2$ ) with a decrease in  $x$ . In the fast frame, AJM configurations are equivalent to the presence of local (in rapidity) color screening of  $q\bar{q}$  pairs in the small  $x$  nucleon wave function [88].

The observed soft  $x_{\mathcal{P}}$  dependence of diffraction is natural in the QCD AJM in the kinematic range of the validity of the DGLAP approximation.

The approximate soft factorization (Eq. 78) is natural in the ladder models of the Pomeron since in these models, the structure of the ladder does not depend on the rapidity for  $\alpha_{\mathcal{P}}(0) \approx 1$ . An increase of the probability of hard small  $x$  processes would result in breaking of the soft factorization at very small  $x_{\mathcal{P}}$ .

At sufficiently small  $x$  and moderate  $Q^2$ , the hard contribution may become significant. Attempts to incorporate these higher twist contributions were taken in a number of the dipole models of the  $\gamma^*N$  interactions (see, e.g., [89] and references therein). However, most of these models ignore the  $Q^2$  evolution of the AJM component.

To conclude, the significant cross section of diffraction in DIS is another demonstration of the important role of color fluctuations in the virtual pho-

ton wave function and of the dominance of soft Pomeron physics even in seemingly hard processes. In such processes soft dynamics together with  $Q^2$  evolution gives a significant contribution to the total cross section.

## 7 Hard Exclusive Processes

### 7.1 Introduction

It has been understood since nearly two decades ago that a number of two-body and quasi two-body processes off nucleons, nuclei, photons, etc. can be legitimately calculated in QCD in the kinematics of fixed  $x$  and  $Q^2 \rightarrow \infty$  as a consequence of the QCD factorization theorem:  $\pi + T \rightarrow 2 \text{ jets} + T'$  [62];  $\gamma_L^* + N \rightarrow V(\rho, J/\Psi, \rho', \dots) + N'$  [34], (where the excitation energy of the state  $T' \ll Q$ );  $\gamma_L^* N \rightarrow \text{Meson}(\pi, K, \eta, \dots) + \text{Baryon}$  [56];  $\gamma_L^* \rightarrow [\text{Few meson system}] + \text{Baryon}$  [56];  $\gamma^* + N \rightarrow \gamma + N$  [90, 91, 92, 88, 93, 94, 95, 96]; and  $\gamma^* + \gamma \rightarrow \text{Meson} + \text{Meson}'$  [97]. These processes provide new ways to investigate the three-dimensional partonic structure of nucleons (transverse distribution of partons with a given light-cone fraction) and to compare it to that of  $\Delta$ -isobars, hyperons, and  $N\pi$ . A theoretical analysis of these processes allows one also to address such novel questions of short-range parton correlations in nucleons as: What is the probability to find a small color singlet cluster in the nucleon made of a quark-antiquark pair, three quarks or even three antiquarks? These processes also probe the minimal light-cone  $q\bar{q}$  components of various mesons and few meson systems. In addition, these processes provide an effective probe of high energy dynamics of QCD and test whether/at what energies the strength of the interaction of small dipoles with nucleons/nuclei reaches the maximal strength allowed by unitarity, which leads to breakdown of the DGLAP QCD evolution equations.

An investigations of the same processes off nuclear targets reveals another distinctive property of QCD: at fixed  $x$  and  $Q^2 \rightarrow \infty$ , nuclear matter is completely transparent to the propagation of spatially small colorless clusters of quarks and gluons—this regime is usually referred to as color transparency. In this limit, the complete transparency for hard diffractive processes unambiguously follows from basic properties of the QCD evolution equations [81]. The observation of color transparency of nuclear matter is the striking confirmation that the interaction in QCD is due to the color charge that is screened within such clusters. Such a phenomenon would be absent, if high energy

processes were dominated by exchanges of usual mesons, as was assumed before the emergence of QCD as the theory of hadronic interactions.

A characteristic feature of these processes is that the final state contains a particle (few particles) that has small momentum in the target rest frame. Hence to study these processes in the fixed target mode, one needs to design a detector that would be able to (1) detect slow particles (including neutrons) over a large range of laboratory angles, (2) measure momenta of the leading hadrons with high resolution, and (3) operate at high luminosity to reach high enough  $Q^2$ —a challenging, though not impossible, task.

Detection of these reactions in the collider kinematics is somewhat easier since the particles that are slow in the target rest frame fly along the beam direction. Also, it is much easier to select coherent interactions with nuclei. The challenge in the case of these reactions is to reach high enough luminosities—so far only channels with vacuum quantum numbers in the  $t$ -channel were investigated at HERA.

The prediction and discovery of the quarks–gluon configurations in hadrons that weakly interact with a target requires also the presence of configurations in the hadron wave function whose interaction with the target is larger than average (see the discussion in section 6.4).

## 7.2 QCD factorization theorem

### 7.2.1 The statement of the theorem [56]

The starting point for the analysis is the factorization theorem for the process

$$\gamma_L^*(q) + p \rightarrow \text{”Meson”}(q + \Delta) + \text{”Baryon”}(p - \Delta) \quad (82)$$

at large  $Q^2$ , with  $t$  and  $x = Q^2/(2p \cdot q)$  fixed. It asserts that the amplitude has the form of convolution of the three blocks depicted in Fig. 7:

$$\begin{aligned} \mathcal{M} = & \sum_{i,j} \int_0^1 dz \int dx_1 f_{i/p}(x_1, x_2, t, \mu) H_{ij}(x_1/x, Q^2, z, \mu) \phi_j(z, \mu) \\ & + \text{power-suppressed corrections,} \end{aligned} \quad (83)$$

where  $f_{/p}$  is the “generalized parton density” (GPD);  $x_1 - x_2 = x$ ;  $\phi$  is the light-front wave function of the meson;  $H_{ij}$  is the hard-scattering coefficient usefully computable in terms of the powers of  $\alpha_s(Q)$ . The contribution of the

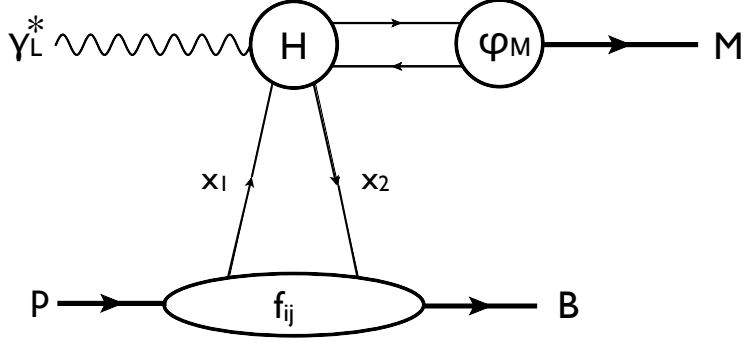


Figure 7: The block structure of the DIS exclusive process  $\gamma_L^* + p \rightarrow$  "meson" + "baryon".

diagrams, where an extra gluon is exchanged between the hard blocks, is suppressed by an additional factor of  $1/Q^2$ . The formal proof [56] is very lengthy so we restrict ourselves in the further discussion by the qualitative explanation only. Qualitatively, the factorization in these processes is due to the color screening/transparency: the small transverse size of  $\gamma_L^*$  selects small-size (point-like) configurations ( $b \sim 1/Q$ ) in the meson and the interaction with such "white" configurations is suppressed by the factor of  $1/Q^2$ . The relation of the color screening to factorization is best seen in the Breit frame. Before the interaction,  $\gamma_L^*$  is static, while after the photon is absorbed, the quark-gluon system (which would form the meson) moves with a large velocity in the direction of the photon keeping the small transverse size, while the baryon system rapidly moves in the opposite direction. No soft interactions between the left and right movers is possible, provided that the meson system has a small transverse size. The same argument is likely to work for the processes where a forward (anti)baryon is produced:  $\gamma_L^* + p \rightarrow$  forward  $N + \pi$ ,  $\gamma_L^* + p \rightarrow$  forward  $\Lambda + K^+$ , and  $\gamma_L^* + p \rightarrow$  forward  $\bar{p} + NN$  [98], though no formal proof has been given so far.

In the case of the transverse polarization of  $\gamma^*$ , the non-perturbative QCD contribution is only suppressed by the power of  $1/\ln Q^2$  (similar to the case of  $F_{2N}(x, Q^2)$ ). It originates from the contribution of highly asymmetric  $q\bar{q}$  pairs in the  $\gamma_T^*$  wave function which have the transverse size similar to that of hadrons.

### 7.2.2 Definitions of light-cone distributions and amplitudes: longitudinally polarized vector meson

*The wave function of longitudinally polarized vector meson.*

The light-cone wave function of a longitudinally polarized vector meson is

$$\phi_j^V(z, \mu^2) = \frac{1}{\sqrt{2N_c}} \int_{-\infty}^{\infty} \frac{dy^+}{4\pi} e^{-izp^-y^+} \langle 0 | \bar{\psi}(y^+, 0, \mathbf{0}_T) \gamma^- \mathcal{P} \psi(0) | V \rangle, \quad (84)$$

where  $\mathcal{P}$  is a path-ordered exponential of the gluon field along the light-like line joining the quark operators entering the matrix element.

*Quark density of the nucleon:*

For a quark of flavor  $i$ , its density in the nucleon ( $q_i$ ) reads:

$$f_{i/p}(x_1, x_2, t, \mu) = \int_{-\infty}^{\infty} \frac{dy^-}{4\pi} e^{-ix_2p^+y^-} \langle p' | T \bar{\psi}(0, y^-, \mathbf{0}_T) \gamma^+ \mathcal{P} \psi(0) | p \rangle \quad (85)$$

Note that in the case of charged mesons,  $i$  stands for the flavor indices of the initial and final quarks.

*Gluon density of the nucleon:*

For the gluon density in the nucleon, one can give the definition symmetric with respect to the  $x_1 \rightarrow x_2$  transposition:

$$\begin{aligned} f_{g/p}(x_1, x_2, t, \mu) &= - \int_{-\infty}^{\infty} \frac{dy^-}{2\pi} \frac{1}{x_1 x_2 p^+} e^{-ix_2p^+y^-} \\ &\times \langle p' | T G_{\nu}^{+}(0, y^-, \mathbf{0}_T) \mathcal{P} G^{\nu+}(0) | p \rangle. \end{aligned} \quad (86)$$

Note that the factor of  $1/(x_1 x_2)$  cancels the inverse factor that appears in the derivative part of the product of the two gluon field strength tensors  $G_{\nu}^{+}(0, y^-, \mathbf{0}_T) G^{\nu+}(0)$ . The normalization condition is

$$x f_{g/p}(x, x, t = 0, \mu) = f_{g/p}(x, \mu), \quad (87)$$

where  $f_{g/p}(x, \mu)$  is the usual (diagonal) gluon PDFs. An additional factor of  $x$  reflects the difference of the symmetric definition of the gluon correlation function from that in the diagonal case.

The  $t$  dependence of the gluon GPDs in the “diagonal” case of  $x_1 = x_2$  is of special importance for the interpretation of various hard  $pp$  processes (see the discussion in section 7.5). It is described by the normalized two-gluon form factor  $F_g(x, t, Q^2)$ , where  $t = -\Delta_\perp^2$  is the transverse momentum transfer to the target. Its Fourier transform describes the transverse spatial distribution of gluons with given  $x$ :

$$F_g(x, \rho|Q^2) \equiv \int \frac{d^2\Delta_\perp}{(2\pi)^2} e^{i(\Delta_\perp\rho)} F_g(x, t = -\Delta_\perp^2|Q^2), \quad (88)$$

where  $\rho \equiv |\rho|$  measures the distance from the transverse center of momentum of the nucleon. The distribution is normalized such that  $\int d^2\rho F_g(x, \rho|Q^2) = 1$ . The information on  $F_g(x, t, Q^2)$  that can be extracted from the hard exclusive processes like  $\gamma + p \rightarrow J/\psi + p$ :

$$F_g(x, q_t^2, Q^2) = 1/(1 - t/m_g^2)^2 \quad (89)$$

Here  $m_g$  is  $\approx 1\text{GeV}$  and slowly decreases with  $x$  decrease.

Modifications necessary for the case of pseudo-scalar meson electroproduction are given in [56].

The GPDs are different from zero for

$$-1 \leq x_1 \leq 1, \quad -1 \leq x_2 \leq 1. \quad (90)$$

There are two physically different regions. In region I,  $x_1 \geq 0$  and  $x_2 \geq 0$ . It corresponds to the knockout of a parton with the light-cone fraction  $x_1$  of the initial target momentum and its absorption in the final state with the light-cone fraction  $x_2$ . The  $Q^2$  evolution is described by the DGLAP-type evolution equations. In the  $x \rightarrow 0$  limit, a simple connection with the diagonal distributions holds. In region II,  $x_1 \geq 0$  and  $x_2 \leq 0$ . This corresponds to scattering off a small-size color singlet ( $\bar{q}q, gg$ ) emitted by the target. The  $\bar{q}q$  case is loosely analogous to scattering off the meson cloud of the target, provided the meson is collapsed into a small-size configuration. In this case, the  $Q^2$  evolution is similar to the one for the meson wave function and is governed by the Brodsky–Lepage–Efremov–Radyushkin evolution equation [99].

The imaginary part of the scattering amplitude originates from region I. Using a dispersion representation in energy, it is possible to calculate the real part of the amplitude for small  $x_{bj}$  and to avoid the consideration of region



II. Secondly, at small  $x_{bj}$ , the space–time evolution of the processes allows for a simpler visualization of the interaction process. Also, most of the currently available data at large  $Q^2$  were obtained at HERA for the small- $x$  kinematics. Thus, as a next step, we summarize the small  $x$ -theory and compare it with the data.

## 7.3 Hard diffractive production of vector mesons

### 7.3.1 Space–time evolution of high energy processes

Vector meson production at small  $x$  in the target rest frame can be described as a three-stage process [34]:

(i) The longitudinally polarized virtual photon  $\gamma_L^*$  with the four-momentum  $q = (zq_0, k_t)$  breaks up into  $\bar{q}q$  with the lifetime (which follows from the energy–time uncertainty principle):

$$\tau_i = l_{\text{coh}}/c = \frac{2q_0}{Q^2 + \frac{k_t^2 + m_q^2}{z(1-z)}} \approx \frac{1}{m_N x}. \quad (91)$$

The coherence length is  $l_{\text{coh}} \geq 100$  fm at HERA.

(ii) The  $\bar{q}q$  pair then scatters off the target proton.

(iii) The  $q\bar{q}$  pair then lives for the time

$$\tau_f = l_f/c = \frac{2q_0}{\frac{k_t^2 + m^2}{z(1-z)}} \quad (92)$$

before the final state vector meson is formed. We note that  $\tau_f \geq \tau_i$ .

As a result, the production amplitude  $A(\gamma_L^* + p \rightarrow V + p)$  can thus be written as convolution of the light-cone wave function of the photon,  $\Psi_{\gamma^* \rightarrow |q\bar{q}\rangle}$ , the scattering amplitude of the hadron state,  $A(nT)$ , and the wave function of the vector meson,  $\psi_V$ :

$$A = \Psi_{\gamma_L^* \rightarrow |n\rangle}^\dagger \otimes A(nT) \otimes \Psi(q\bar{q} \rightarrow V). \quad (93)$$

In the impact parameter space:

$$A = \int d^2b \psi_{\gamma_L^*}(b) \sigma(b, s) \psi_V(b), \quad (94)$$

where  $b$  is the transverse separation of  $q$  and  $\bar{q}$ .

The leading twist expression is [34]:

$$\left. \frac{d\sigma_{\gamma^* N \rightarrow VN}^L}{dt} \right|_{t=0} = \frac{12\pi^3 \Gamma_{V \rightarrow e^+e^-} M_V \alpha_s^2(Q) \eta_V^2 \left| \left(1 + i\frac{\pi}{2} \frac{d}{d \ln x}\right) x G_T(x, Q^2) \right|^2}{\alpha_{EM} Q^6 N_c^2}. \quad (95)$$

Here,  $\Gamma_{V \rightarrow e^+e^-}$  is the decay width of  $V \rightarrow e^+e^-$  and

$$\eta_V \equiv \frac{1}{2} \frac{\int \frac{dz d^2 k_t}{z(1-z)} \Phi_V(z, k_t)}{\int dz d^2 k_t \Phi_V(z, k_t)} \rightarrow 3 \quad (96)$$

for  $Q^2 \rightarrow \infty$ . The rapid onset of the leading twist formulas for  $\sigma(e\bar{e} \rightarrow \text{hadrons})$  suggests that for  $\rho$  and  $\phi$  mesons,  $\Phi_V(z, k_t)$  and hence  $\eta$  are already close to the asymptotic value at  $Q^2 \sim$  a few  $\text{GeV}^2$ .

Note here that in this expression, the difference between the light-cone fractions  $x_1$  and  $x_2$  was neglected. For large  $Q^2$ , the non-diagonal GPD is calculable [100, 101] through the diagonal one since the DGLAP evolution for GPDs conserves  $x = x_1 - x_2$ , while the light-cone fractions essential at the starting point of the evolution grow with an increase of  $Q^2$ .

In [102] elastic photoproduction of  $J/\psi$  was evaluated in the leading  $g^2 \ln(x_0/x)$  approximation. As we discussed above this approximation ignores huge NLO effects.

At extremely small values of  $x$ , that are significantly smaller than those characteristic for the applicability of the DGLAP approximation, the  $\ln(x_0/x)$  terms not enhanced by  $\ln(Q^2/Q_0^2)$  and thus neglected in the DGLAP approximation, become important. The restriction on the region of applicability leading  $\log(x_0/x)$  approximation follows from the necessity to take into account energy-momentum conservation. Indeed, in multi-Regge kinematics, the interval in rapidity between adjacent radiations within the ladder is  $\Delta y \gg 2$ . This number is comparable with the interval in rapidities achieved (to be achieved) in DIS:

$$\Delta y = \ln(1/x) + 2 \ln(Q/m_N). \quad (97)$$

For the edge of the kinematics achieved at HERA,  $\Delta y \approx 10$ . Since four units of rapidity are occupied by the two fragmentation regions, two-to-three gluons are allowed to be radiated in this kinematics. This is insufficient for the dominance of multi-Regge kinematics characteristic for LL approximation. So far there have been no attempts to describe hard diffractive processes

in the resummation approach. Note that formulas obtained in the double logarithmic approximation,  $\alpha_s \ll 1$  and  $\alpha_s \ln(x_0/x) \ln(Q^2/Q_0^2) \sim 1$ , should coincide for the BFKL and DGLAP approximations.

### 7.3.2 Modeling finite- $Q^2$ effects

In the convolution integral (Eq. 93),  $\Psi_{\gamma^*}^L(b)$  with  $b \propto \frac{1}{Q}$  is convoluted with the broad wave function of a light vector meson<sup>2</sup>. Hence, the average distances contributing to  $\sigma_L$  are significantly smaller than those contributing to  $\sigma_T$ . As a result, the effective  $Q^2$  is smaller for vector meson production than for  $\sigma_L$  [103] (Fig. 8). This effect is taken into account by evaluating  $\sigma(q\bar{q} - N)$  using the dipole model. One also has to include the difference between  $x_1$  and  $x_2$ , which is absent when the dipole model is applied to inclusive DIS.

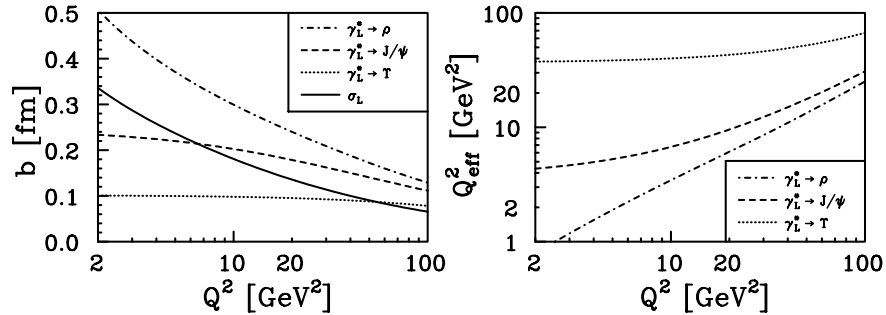


Figure 8: The dependence of the average  $b$  (left) and the effective  $Q^2$  (right) on  $Q^2$  for production of vector mesons [103].

A related effect is that, at pre-asymptotic energies, one cannot substitute  $\Psi_V(b)$  by  $\Psi_V(0)$ . This higher twist correction leads to the suppression of the amplitude by the factor:

$$T(Q^2) = \frac{|\int d^2b dz \Psi_{\gamma_L^*}(z, b) \sigma(q\bar{q} - N) \phi_V(z, b)|^2}{|\int d^2b dz \Psi_{\gamma_L^*}(z, b) \sigma(q\bar{q} - N) \phi_V(z, 0)|^2}. \quad (98)$$

The HERA data (for a recent summary, see [29]) have confirmed the following basic predictions of pQCD [34]:

<sup>2</sup>To obtain this expression, one needs first to apply conservation of the electromagnetic current to express the bad component of the current through the good one.

- The rapid increase with energy— $|xG_N(x, Q_{\text{eff}}^2)|^2 \propto W^{0.8}$  for  $Q_{\text{eff}}^2 \sim 4$  GeV<sup>2</sup>—of  $\rho$  production for  $Q^2 = 10 - 20$  GeV<sup>2</sup> and of  $J/\psi$  production for  $Q^2 \leq 10$  GeV<sup>2</sup>. (Note that  $\sigma(W) \propto W^{0.32}$  for soft physics at  $t = 0$  and is even slower for the cross section integrated over  $t$ .) For  $\Upsilon$  production,  $Q_{\text{eff}}^2 \approx 40$  GeV<sup>2</sup> which leads to  $\sigma(W) \propto W^{1.7}$ . This prediction maybe tested in the ultraperipheral collisions at the LHC [104].
- The absolute values of the cross sections of vector meson production are well reproduced, provided that the factor  $T$  (Eq. 98) is taken into account. In the case of  $\Upsilon$  photoproduction, the skewedness effects due to large difference between  $x_1$  and  $x_2$  as well as the large value of the real part of the amplitude are important. Together they increase the predicted cross section by a factor of about four [105, 106].
- The decrease of  $\sigma_L$  with  $Q^2$  is slower than  $1/Q^6$  because of the  $|\alpha_S G_N|^2$  and  $T(Q^2)$  factors.
- The ratio  $\sigma_L/\sigma_T \gg 1$  for  $Q^2 \gg m_V^2$ .
- There is a universal  $t$  dependence for large  $Q^2$  originating solely from the two-gluon–nucleon form factor. The model, which takes into account squeezing of  $\gamma_L$  with  $Q^2$ , provides a reasonable description of the convergence of the  $t$ -slopes of light mesons and  $J/\psi$  production and makes the observation that the slope of  $J/\psi$  production is practically  $Q^2$  independent (Fig. 9).

### 7.3.3 Lessons and open problems

- Transition from soft to hard regime.

We can estimate the effective size of a  $q\bar{q}$  dipole as

$$\frac{B(Q^2) - B_{2g}}{B(Q^2 = 0) - B_{2g}} \sim \frac{R^2(\text{dipole})}{R_\rho^2}, \quad (99)$$

where  $B_{2g}$  is the slope of the square of the two-gluon form factor. Based on the HERA data [108], we conclude that

$$R^2(\text{dipole})(Q^2 \geq 3 \text{ GeV}^2)/R_\rho^2 \leq 1/2 - 1/3 \quad (100)$$

for collider energies. Accordingly, it appears that the soft energy dependence of the cross section persists over a significant range of the dipole sizes. (This

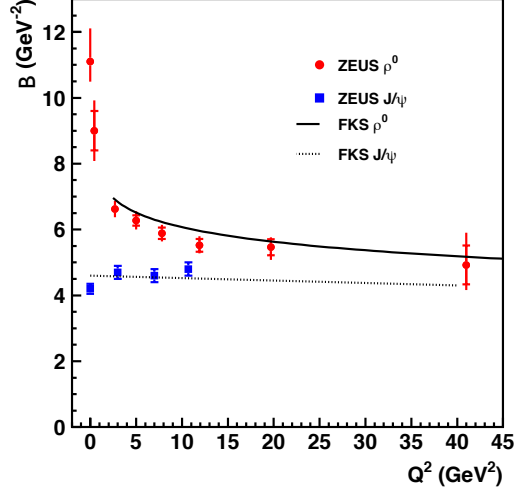


Figure 9: The convergence of the  $t$ -slopes,  $B$ , of  $\rho$  and  $J/\psi$  electroproduction at high  $Q^2$ . The data are from [107, 108]; the curves are the predictions of [103].

is consistent with the observed similarity of the energy dependence of  $\rho$  and  $\phi$  photoproduction.)

- In the pQCD regime, the  $t$ -slope the dipole–nucleon amplitude should be a weak function of  $s = W^2$ ,  $B(s) = B(s_0) + 2\alpha'_{\text{eff}} \ln(s/s_0)$ , since the Gribov diffusion in the hard regime is small (see the discussion in section 4). Hence, a significant contribution to  $\alpha'$  comes from the variation of the  $t$  dependence of the gluon GPD with an decrease in  $x$  at  $Q_0^2$ .

- The contribution of soft QCD physics in the overlapping integral between the wave functions of the virtual photon and the transversely polarized vector meson is suppressed by the Sudakov form factor (see, e.g., the discussion in [109]), which is absent in the case of the processes initiated by longitudinally polarized photons. This is probably relevant for the understanding of similar dependence of  $\sigma_{L,T}$  on  $x$  and on  $t$  that were observed at HERA.

## 7.4 Meson production at intermediate $x$

An analysis of the HERA data on vector meson production indicates that, up to rather large  $Q^2$ , cross sections of hard exclusive processes are suppressed significantly as compared to the leading twist QCD predictions. The origin of this is higher twist effects originating from the contribution of the transverse sizes that are comparable in the longitudinal photon and the meson wave functions.

At the same time, the overall transverse size of the produced meson is quite small ( $\leq 0.4$  fm) already for  $Q^2 \geq 5$  GeV<sup>2</sup>. Due to the color transparency phenomenon, this leads to a strong suppression of the final state interaction of the  $q\bar{q}$  pair, which in the end will fragment into the meson and the residual baryon system. For  $W \leq 20$  GeV, this cross section is of the order of few mb. Besides, the expansion of the  $q\bar{q}$  system to a normal hadron size in the nucleon rest frame takes a significant distance

$$l_{coh} \sim 2p_M/(\Delta m_M^2) \sim \frac{1}{xM_N}Q^2/(\Delta m_M^2) \quad (101)$$

where  $\Delta m_M^2 \leq 1$  GeV<sup>2</sup>, and  $(\Delta m_M^2)/2p_M$  is the characteristic light-cone energy denominator for a meson  $M$ . The condition  $l_{coh} \gg r_N$  is satisfied for  $x \leq 0.2$  already for  $Q^2 \geq 5$  GeV<sup>2</sup>. Hence, it seems likely that the precocious factorization into the three blocks (Fig. 7)—the overlap integral between the photon and the meson wave functions, the hard blob, and the skewed distribution—could be valid already at moderately high  $Q^2$ , leading to precocious scaling of the spin asymmetries and of the cross section ratios as a function of  $Q^2$ .

The discussion of numerous promising channels such as production of charged and neutral vector mesons ( $\rho^{\pm,0}$ ,  $K^{*+}$ , ...), pseudoscalar mesons  $\pi^0, \eta, \eta'$  that are sensitive to the QCD axial anomaly, and  $\Delta$ -isobars is beyond the scope of this review (for a detailed discussion, see [110]).

## 7.5 Transverse structure of the nucleon at small $x$ from GPDs

At small  $x$  many processes are dominated by the two-gluon ladder with no contribution from quark GPDs—like production of  $J/\psi$  and  $\Upsilon$ . In the case of GPDs linked to sea quarks, the situation is more complicated. In the case of the deeply virtual Compton scattering (DVCS) amplitude in the NLO

approximation, quark and gluon contributions enter with opposite signs and are of a comparable magnitude [111]. As a result, a relatively small difference of the transverse sizes of the sea quarks and gluons, which is expected due to pionic cloud effects [112], is amplified in the  $t$ -slope of DVCS. Thus, precision measurements of the quark GPDs at small  $x$  require an accurate measurement of the gluon GPD.

Higher twist (HT) effects modify the  $t$ -distribution of light mesons up to  $Q^2 \sim 15 \text{ GeV}^2$ . Therefore, it appears that the only practical chance to perform a precision measurement of the gluon GPDs is the production of onium states.

The effects of non-diagonality in the gluon GPD appear to be small for the  $J/\psi$  case, this is due to the large transverse momenta in the wave function, which lead to the comparable light-cone fractions of the gluons attached to  $c\bar{c}$ :  $x_1/x_2 \sim 2$ ,  $x_1 - x_2 = x = (Q^2 + m_{J/\psi}^2)/W^2$ . In the  $\Upsilon$  case, the effect of non-diagonality can be taken into account via the DGLAP evolution. As a result,

$$\frac{d\sigma^{\gamma+p \rightarrow J/\psi+p}}{dt} \propto F_g^2(x, t) \exp(\Delta B t), \quad (102)$$

where  $F_g(x, t)$  is the two-gluon form factor of the nucleon; the second factor takes into account a small but finite correction due to the finite size of  $J/\psi$  that was estimated in [103] to be  $\Delta B \approx 0.3 \text{ GeV}^{-2}$ .

The  $t$ -dependence of the measured differential cross sections of exclusive processes for  $|t| < 1 \text{ GeV}^2$  is commonly described either by an exponential or by a dipole form inspired by analogy with the nucleon elastic form factors. The data are not precise enough to distinguish between the two forms since they mostly differ at small  $t$ , where the resolution of the measurements is moderate, and at large  $-t \geq 0.8 \text{ GeV}^2$ , where the measurements rather strongly depend on the procedure of subtraction of the inelastic background contribution.

The data can be fitted in the following form [113]:

$$B_g(x) = B_{g0} + 2\alpha'_g \ln(x_0/x), \quad (103)$$

where

$$x_0 = 0.001, \quad B_{g0} = 4.1 \text{ }^{(+0.3)}_{(-0.5)} \text{ GeV}^{-2}, \quad \alpha'_g = 0.140 \text{ }^{(+0.08)}_{(-0.08)} \text{ GeV}^{-2}. \quad (104)$$

Fits of similar quality are produced with the dipole form:

$$F_g(x, t|Q^2) = (1 - t/m_g^2)^{-2}, \quad B_g = 3.2/m_g^2 \text{ (for } m_g^2 \sim 1 \text{ GeV}^2). \quad (105)$$

The spatial distributions of gluons in the transverse plane corresponding to the two fits are:

$$F_g(x, \rho|Q^2) = \begin{cases} (2\pi B_g)^{-1} \exp[-\rho^2/(2B_g)], \\ [m_g^2/(2\pi)] (m_g\rho/2) K_1(m_g\rho), \end{cases} \quad (106)$$

These transverse distributions are similar for the average  $\rho$ , leading, for example, to the nearly identical distributions over the impact parameter for production of dijets in  $pp$  collisions at the LHC [113]. At the same time, the dipole fit gives a significantly larger  $F_g(x, \rho|Q^2)$  for small  $b$ . As a result, analyses of the proximity to the black disc regime for the interaction of a small dipole with the nucleon for small  $b$  are sensitive to the choice of the model for  $F_g(x, \rho|Q^2)$ . A related effect is a factor of 1.6 difference of  $\langle b_g^2 \rangle$  in the two fits. The conclusion [114] that gluons are localized in a smaller transverse area than that given by the e.m. form factor is based on the use of the same shape for the e.m. and two-gluon form factors.

The current knowledge of  $F_g(x, \rho|Q^2)$  allows us to study the impact parameter dependence of dijet production at collider energies. One finds that the median impact parameters for the inelastic  $pp$  collisions with jet production are a factor of two smaller than those for the minimal bias inelastic events, and weakly depend on the rapidity and  $p_t$  of the jets. This may explain the regularities in the multiplicity of the underlying events on  $p_t$  of the trigger [113]. It also provides an important constraint for the models of inelastic  $pp$  collisions at the LHC and, in particular, of the dynamics of multiparton interactions.

## 7.6 Break-up processes with gaps: from small to large $t$

### 7.6.1 Probing fluctuations of the gluon field

In the high energy  $\gamma^* + p \rightarrow M + \text{rapidity gap} + X$  process, at  $t \approx 0$  the two-gluon ladder couples only to one parton in the target in the leading twist approximation. If the strength of the coupling to all configurations containing partons with a given  $x$  were the same, it would be impossible to produce an inelastic final system  $X$ . As a result, similarly to the case of inelastic diffraction of hadrons off hadrons, the discussed process measures the variance of the gluon field. It is given by the ratio of the diffraction dissociation and elastic cross sections for vector meson production at  $t =$



0 [115]:

$$\omega_{\text{hard}} = \frac{d\sigma^{\gamma^*+p \rightarrow V+\text{rapidity gap}+M_X}(x, Q^2)/dt}{d\sigma^{\gamma^*+p \rightarrow V+p}(x, Q^2)/dt} = \frac{\langle G^4 \rangle - \langle G^2 \rangle^2}{\langle G^2 \rangle^2}. \quad (107)$$

Our estimates of the strength of the fluctuations due to the fluctuations of the overall size of the nucleon, as seen in soft inelastic diffraction, find that  $\omega_{\text{hard}} \approx 0.15$  at small  $x$ , which is consistent with the current data.

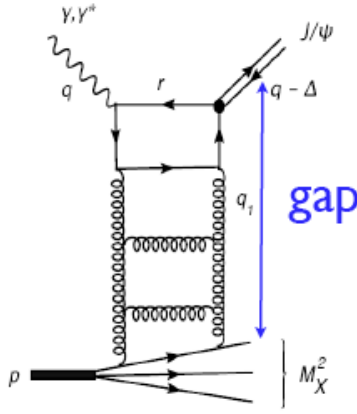


Figure 10: A typical QCD diagram for the rapidity gap process (108).

### 7.6.2 Onset of new regime at large $t$

In order to determine the spacial distribution of gluons at  $b \sim 0$ , one needs to study exclusive processes at large  $t$  since in this case the integral over  $-t$  in the Fourier transform converges very slowly. For example, in the case of the dipole fit, half of the contribution to  $F_g(x, b = 0)$  originates from  $-t \geq m_g^2$  and one quarter, from  $-t \geq 3m_g^2$ . This implies that one needs a detector which will be able to separate exclusive processes from diffractive dissociation in a very broad range of  $t$ , where the dissociation dominates by far.

A further complication is that the QCD factorization theorem [56] was derived in the limit of  $t = \text{const}$ ,  $x = \text{const}$ , and  $Q^2 \rightarrow \infty$ . Recent studies [33] found that the pattern of the QCD evolution changes in the kinematical domain when  $-t$  becomes comparable to the intrinsic hardness scale of the

process ( $Q_{\text{eff}}^2 \sim 3 \text{ GeV}^2$  for  $J/\psi$  photoproduction). The DGLAP equations require modifications in this case. Let us, for example, consider the process

$$\gamma^* + p \rightarrow J/\psi + \text{rapidity gap} + M_X \quad (108)$$

for large  $-t$ , which is still smaller than  $Q^2 + M_{J/\psi}^2$ . The typical leading QCD diagrams (Fig. 10) correspond to the attachment of the two-gluon ladder to a parton with  $x_J = -t/(-t + M_X^2 - m_N^2)$ . The cross section has the factorized form similar to [116]:

$$\frac{d\sigma_{\gamma+p \rightarrow V+X}}{dt dx_J} = \frac{d\sigma_{\gamma+\text{quark} \rightarrow V+\text{quark}}}{dt} \left[ \frac{81}{16} g_p(x_J, t) + \sum_i (q_p^i(x_J, t) + \bar{q}_p^i(x_J, t)) \right]. \quad (109)$$

At fixed  $x_j$ , the energy dependence is determined by the evolution of the dipole-parton elastic scattering amplitude with  $x/x_J$ . In difference from the small  $t$  limit, the DGLAP evolution is strongly suppressed and completely disappears for  $-t$  close to the intrinsic scale. The HERA data [117] on the energy dependence of the process (108) are consistent with the behavior expected in QCD.

Consequently, the effective  $\alpha_{\mathcal{P}}(t)$  in this limit stays close to unity until very small  $x/x_J$  (not available at HERA) where the Pomeron-type behavior may reveal itself.

The same mechanism may be responsible for part of the drop of  $\alpha_{\mathcal{P}}(t)$  with an increase in  $-t$  observed for elastic  $J/\psi$  production. This may indicate that precision measurements of the  $t$  dependence of the two-gluon form factor at high energies would require using of electroproduction rather than of photoproduction. The discussed phenomenon may also be relevant for the explanation of the pattern observed in photoproduction of  $\rho$  mesons, where  $\alpha_{\mathcal{P}}(t)$  appears to flatten out around  $\alpha_{\mathcal{P}}(t) = 1$  for large  $|t|$  (Fig. 3).

### 7.6.3 Probing minimal quark component in the pion

The QCD factorization theorem discussed in the previous subsections allows us to calculate another group of hard processes where the selection of the final state dictates squeezing of the initial state. This is a particular case of the pre-selection phenomenon familiar from non-relativistic quantum mechanics. The most straightforward process is

$$\pi + T \rightarrow \text{two jets} + \text{rapidity gap} + T. \quad (110)$$

This process is in a sense a mirror image of vector meson production in DIS. The pion in the initial state collapses into a small-size configuration due to the hard interaction; this  $q\bar{q}$  pair interacts coherently with the target and transforms into two jets [62] (Fig. 11).

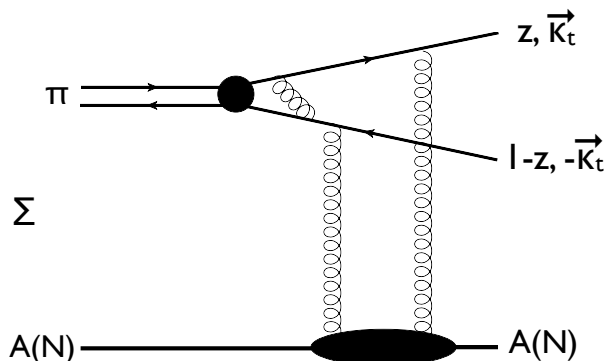


Figure 11: A typical two-gluon ladder exchange diagram contributing to the process of pion coherent diffractive dissociation.

In the limit of large transverse momenta of the jets, one can justify applicability of the QCD factorization theorem and obtain [118]:

$$\frac{d\sigma(\pi + A \rightarrow 2jet + A)(q_t = 0)}{dt dz d^2\kappa_t} = \frac{(1 + \eta^2)}{16\pi(2\pi)^3} \left[ \Delta(\chi_\pi(z, \kappa_t)) \frac{\alpha_s \pi^2}{3} x_1 G_A(x_1, x_2, Q^2) \right]^2, \quad (111)$$

where  $\chi_\pi(z, \kappa_t) \equiv 4\pi C_F \frac{\alpha_s(\kappa_t^2)}{\kappa_t^2} \sqrt{3} f_\pi z(1-z)$ ;  $\Delta$  is the Laplacian in the  $\kappa_t$  space;  $z$  is the fraction of the light-cone plus-momentum carried by the quark in the final state;  $x_1 G_A(x_1, x_2, \kappa_t^2)$  is the generalized gluon density of the nucleus, where  $x_1$  and  $x_2$  are the fractions of the target momentum carried by exchanged gluons 1 and 2 respectively,  $x_1 - x_2 = M_{2jet}^2/s$  and  $x_2 \leq x_1$  and the integral over  $x_2$  is not written explicitly;  $\eta = \text{Re}F/\text{Im}F$ , where  $F$  as the dipole–nucleon scattering amplitude). Note that the resulting  $\kappa_t^{-8}$  dependence is a consequence of the comparatively well-understood wave function of the pion. This wave function determines the asymptotic behavior of the pion electromagnetic form factor.

For  $x \geq 0.03$ ,  $G_A(x, Q^2) = AG_N(x, Q^2)$ . Hence, for this kinematics there are no absorptive effects—the amplitude at  $t = 0$  should be  $\propto A$ . This prediction has been confirmed at FNAL with  $p_\pi=500$  GeV/c: the experiment [119]

observed a strong coherent peak for dijet production from carbon and platinum targets and measured the  $A$  dependence for this interval of  $A$  that was found to be  $A^{1.54}$ . The ratio of the cross sections for the two targets is a factor of seven larger than that for soft coherent diffraction. Furthermore, the observed dependence of the cross section on the pion momentum fraction and the jet transverse momentum is well-consistent with the perturbative QCD prediction of [62, 118] for  $k_t \geq 1.5$  GeV/c. The relatively early onset of scaling for this process—as compared to diffractive electroproduction of vector mesons discussed above—maybe due to the presence of the plane wave in the convolution formula for the dijet production cross section. This should be compared to the case of the virtual photon wave function that restricts the phase space much stronger.

We would like to note that the derivation of the QCD factorization theorem for this process [118] heavily used the fact that the trigger on two high- $\kappa_t$  jets along with the Ward identities enforce the  $q\bar{q}$  pair and, therefore, the color to be concentrated in the interaction volume  $\propto 1/\kappa_t^2$ . The use of the asymptotic freedom and the restriction by the leading twist contribution guarantees the dominance of the  $q\bar{q}$ -component in the pion wave function at sufficiently large  $\kappa$ . The generalized gluon distribution of the target depends on variables  $x_1 \gg x_2$  and  $x_1 - x_2 = M_{2\text{jet}}^2/s$ . The kinematics follows from energy–momentum conservation. The mass of the two jets,  $M_{2\text{jet}}$ , is significantly larger than the pion mass; that allowed one to justify the applicability of pQCD and the Ward identities. The calculation also explores the asymptotic solution of the QCD evolution equation for the pion wave function.

It was assumed in [120] that for the calculation, one can substitute the pion by a system of the non-interacting quark and antiquark with the mass equal that of the two-jet system  $M_{2\text{jet}} \gg m_\pi$ . This assumption violates the conditions of the applicability of the QCD factorization theorem discussed above and, therefore, produces a different amplitude. There is no requirement for the  $q\bar{q}$  pair (color) to be within a small volume. Therefore, there is no way to justify the applicability of pQCD and to neglect other quark–gluon configurations. The calculation of leading Feynman diagrams due to the two-gluon exchange produces the factor  $1/(M_{2\text{jet}}^2 - M_\pi^2)$ , while in the kinematics of [120],  $M_i = M_{2\text{jet}}$ . A prescription is needed to remove this artificial singularity. Violation of the Ward identities requires an additional prescription of how to derive the condition that the leading amplitude for  $q\bar{q}$  scattering off the two-gluon ladder exchange is  $\propto r_t^2$ , where  $r_t$  is the

momentum of the exchanged gluon. In this kinematics,  $x_1 = x_2 \approx 0$ . Besides, in the framework of the approximations discussed above, the authors [120] found that the scattering amplitude contains singularities that contradict the Landau rules for the amplitudes of physical processes.

For a proton projectile, the related process would be proton diffraction into three jets:

$$p + A \rightarrow \text{three jets} + \text{rapidity gap} + A. \quad (112)$$

So far, the observation of this process at the LHC looks very difficult—current detectors do not have acceptance for realistic  $p_t$  of jets of this process.

## 7.7 Nuclear effects in hard exclusive reactions

The use of nuclear targets provides complementary probes of the QCD dynamics of diffractive processes. QCD predicts that a sufficiently energetic, spatially small color-neutral wave packet of quarks and gluons should traverse hadron medium without absorption. This prediction is equivalent to the QCD factorization theorem of [56]. The complete transparency of nuclear matter [color transparency (CT)] has been unambiguously observed at several experiments at high energies (see discussion below). Such processes are becoming a promising tool for the detailed investigation of the quark and gluon structure of nuclei.

We give here just a few examples. The factorization theorem [56] predicts for coherent electroproduction of vector mesons [62, 34]:

$$\frac{d\sigma}{dt}(\gamma^* A \rightarrow VA)|_{t=0} = \left[ \frac{F_A^L(x, Q)}{F_N^L(x, Q)} \right]^2 = \frac{G_A^2(x, Q)}{G_N^2(x, Q)} = A^{2\alpha_g(x, Q)}, \quad (113)$$

with  $\alpha_g(x, Q) \approx 1$  for  $x \geq 0.02$ . Thus final-state interaction in this process is a higher twist effect.

- Almost complete transparency has been observed at FNAL [121] in both the coherent and incoherent processes:  $\gamma A \rightarrow J/\Psi + A$ ,  $\gamma A \rightarrow J/\Psi + A^*$ .

- Complete transparency of nuclear matter, which follows from the QCD factorization theorem for the sufficiently large transverse momenta of jets  $k_t \geq 2$  GeV, has been observed in the processes  $\pi + A \rightarrow 2 \text{ jets} + A'$  [119].

- For quasi-elastic scattering off nuclei and for large enough  $|t| \geq 0.1$  GeV<sup>2</sup>, one can use closure over the processes of nuclear disintegration  $A'$ .

For example, for production of neutral mesons, one obtains [98]:

$$\sum_{A'} \frac{d\sigma(\gamma_L^* + A \rightarrow M + A')}{dt} = Z \frac{d\sigma(\gamma_L^* + p \rightarrow M + p')}{dt} + N \frac{d\sigma(\gamma_L^* + n \rightarrow M + n')}{dt}. \quad (114)$$

- The color transparency phenomenon leads to a strong suppression of the cross section of coherent scattering off the lightest nuclei for the  $t$  range, where double scattering dominates [122].

At lower energies, where the Lorentz factor is not large enough to guarantee the sufficiently large lifetime of a spatially small wave packet of quarks and gluons traversing a nuclear target, CT is masked to large extent by the following quantum mechanical phenomenon: the small-size wave packet is not an eigenstate of the QCD Hamiltonian and, hence, it rapidly expands [123].

- The onset of complete transparency has been observed [124] in the incoherent process  $\gamma^* + A \rightarrow \rho + X$  at  $\nu \sim 200$  GeV in the kinematics where hadron production in the nuclear fragmentation region was allowed. A smaller effect was observed at  $\nu \sim 15$  GeV under similar conditions [125].
- A gradual increase of transparency in exclusive processes with an increase of  $Q^2$  was observed in high precision experiments at JLab at  $\nu \sim$  a few GeV that measured production of  $\pi^+$  [126] and  $\rho^0$  [127]. The observed  $A$  and  $Q^2$  dependencies are consistent with the familiar quantum mechanical effect of the expansion of a small  $q\bar{q}$  wave packet with distance [87].

In collider kinematics, it is much easier to check whether the nucleus remained intact and to also select certain exclusive break-up channels. Hence, it may be easier to study color transparency effects for these processes at colliders.

Overall, the use of nuclei would add substantially to the program of studies on hard exclusive processes for the  $x \geq 0.05$  range. Since nuclear parton densities for a wide range of  $x \geq 0.05$  are  $\propto A$  up to a small correction due to the EMC effect, one would not have to deal simultaneously with the effect of leading twist shadowing.

## 7.8 Summary

Hard exclusive meson (few meson) production is calculable in QCD in the same sense as the leading twist DIS processes. Hard exclusive processes provide unique ways to study minimal Fock state components of mesons and structure functions of mesons, to compare skewed parton distributions in a multitude of baryons, and to investigate the onset of color transparency.

Colliders have a number of advantages for observing many of these processes.

To have a successful program of studies on the hadron and nuclear structure in the next decade, one needs a triad of electron accelerator facilities optimized to study the following three  $x$  ranges: (a) the  $x \geq 0.3$  range relevant for the study of short-range correlations in nucleons and nuclei, (b) the  $0.05 \leq x \leq 0.3$  range relevant for the study of multiparton correlations in nucleons and the origin of the nuclear forces, (c) the  $x \leq 0.05$  range relevant for the nuclear shadowing phenomena, high parton density physics, etc. This corresponds well to the  $W \leq 8$  GeV range discussed for the upgrade of the Jefferson Lab facility and for the COMPASS experiment with the recoil detector as well as to the  $W \sim 30 - 150$  GeV range discussed for the electron–nucleon/nucleus colliders at JLab and RHIC and for the LHeC collider at CERN.

# 8 A new regime of high energy QCD

## 8.1 Introduction

At large energies, hard QCD interactions become strong at central impact parameters in spite of the small running coupling constant and a larger scale of momenta. The necessity to take into account an entire series in  $(1/Q^2)^n$  (which resembles the situation in the second-order phase transitions) shows that this new phase of QCD has a different continuous symmetry (conformal symmetry), thereby distinguishing it from the perturbative phase of QCD.

With a further increase of energy, predictions based on the QCD factorization theorems start to contradict probability conservation. For the interaction of a spatially small dipole with a target, this can be formulated as:

$$\sigma_{\text{el}}(\text{dipole} + T) \leq \frac{1}{2} \sigma_{\text{tot}}(\text{dipole} + T). \quad (115)$$

The upper limit on the  $\sigma_{\text{el}}/\sigma_{\text{tot}}$  ratio is reached in the regime of complete absorption for all essential impact parameters. The restriction due to probability conservation is stronger for the scattering at central impact parameters (see the discussion in section 8.2).

In the leading twist approximation, the inequality (115) is violated at sufficiently small  $x$  since the QCD factorization theorem for the interaction of a small-size colorless dipole leads to  $\sigma_{\text{el}} \propto (xG_T(x, Q^2)/Q^2)^2/B$ , which becomes larger than  $\sigma_{\text{tot}} \propto xG_T(x, Q^2)/Q^2$  for sufficiently small  $x$  ( $B$  is the  $t$ -slope of the differential cross section of the dipole–target elastic scattering). Thus, in the limit of fixed and large  $Q^2$ ,  $x \rightarrow 0$  and fixed impact parameters, the decomposition over high powers of  $(1/Q^2)^n$  (over twists) becomes ineffective. Indeed, the dependence of the higher twist term  $T_{n+2}$  on  $x$  and  $Q^2$  can be easily evaluated at large energies:  $T_{n+2} \propto (1/Q^2)^n (x_0/x)^{(1+n)(\lambda-1)}$ . Therefore the ranking over twists disappears at sufficiently small  $x$ . As a result, the concept of a spatially small dipole becomes ineffective as well since the contribution of various higher twist effects (for example, the splitting of a small dipole into two small dipoles each interacting with the target) is not suppressed at these energies. In other words, the effective number of dipoles continuously increases with energy.

The regime of complete absorption at fixed impact parameters and conservation of probability does not preclude a rapid increase in cross sections of hard processes in  $pp$  collisions at central impact parameters as well as of the  $\gamma^*N$  cross section with a decrease in  $x$  at fixed  $Q^2$ . At collider energies, the hard contribution to the nucleon structure functions increases with energy as  $\sigma(\gamma^*N) \propto \ln^2(x_0/x)$ , which is faster than the  $x^{-0.2}$  behavior observed at HERA at  $Q^2 \sim$  a few  $\text{GeV}^2$ . At very high energies, an even faster increase is expected,  $\sigma(\gamma^*N) \propto \ln^3(x_0/x)$  [128, 129]. The additional  $\ln(x_0/x)$  is a consequence of the singular behavior of the light-cone wave function of the virtual photon in the coordinate space, which in the momentum space corresponds to the contribution of the quarks with momenta  $\gg Q$  in the box diagram. Numerical studies on the energy dependence of  $F_{2N}(x, Q^2)$  that took into account the taming of partial waves at small impact parameters, were performed in a number of papers using the dipole model (see, for example, [130]).

Note also that QCD predicts taming of structure functions of nuclei which competes with the nuclear shadowing phenomenon. However, it is hard to observe the violation of the DGLAP approximation by an analysis of the experimental data in the current energy range since the evolution equation



is linear and has the flexible initial condition.

Deep inelastic interactions studied so far at HERA are far from the strong absorption regime for the QCD interactions with a small coupling constant. The only possible exception is the the gluon dipole–nucleon interaction at central impact parameters. However, the situation may change in the case of scattering off heavy nuclei and also in the case of central  $pp/pA/AA$  collisions at the LHC.

## 8.2 Conflict of pQCD with probability conservation.

Asymptotic freedom in pQCD does not guarantee probability conservation since pQCD amplitudes are rapidly increasing with energy. The conflict with probability conservation reveals itself in the scattering of a color singlet wave packet of quarks and gluons of the small diameter  $d$  off a hadron target, see Eq. 115. The cross section of elastic scattering of a dipole off the nucleon target can be parametrized as:

$$\frac{d\sigma_{\text{el}}(\text{dipole} + N \rightarrow \text{dipole} + N)}{dt} = \frac{\sigma_{\text{tot}}(\text{dipole} + N)^2}{16\pi} F_{2g}^2(t), \quad (116)$$

where  $F_{2g}(t)$  is the two-gluon form factor of the nucleon extracted in [114] from the HERA data on hard diffractive electroproduction of  $J/\psi$ . At  $t = 0$ , Eq. 116 is the optical theorem. In the expression above we neglected a small contribution of the real part of the elastic dipole scattering amplitude. Using Eqs. 116 and 115, we obtain the following inequality:

$$\frac{\sigma_{\text{tot}}(\text{dipole} + N)}{16\pi} \int dt F_{2g}^2(t) \leq 1/2. \quad (117)$$

In the case of scattering at the zero impact parameter, the inequality is a factor of  $\sim 2$  stronger:

$$\frac{\sigma_{\text{tot}}(\text{dipole} + N)}{8\pi} \int dt F_{2g}(t) \leq 1. \quad (118)$$

One can also study the unitarity condition as a function of an impact parameter using Eq. 57 [131, 132].

The cross section for a spatially small color singlet dipole scattering off the nucleon target follows directly from the pQCD factorization theorem in the leading  $\alpha_s \ln(Q^2/Q_0^2)$  approximation [61, 62, 63]. It can also be derived from the Born term obtained in the leading  $\alpha_s \ln(x_0/x)$  approximation

in [64]. Using the machinery of pQCD calculations, it should not be too difficult to calculate a series of LO, NLO, and NNLO approximations including corrections to the cross section and to the dipole wave function itself.

Since the expressions in the leading log approximation are too bulky, for illustration purposes, we use the fit  $xG \propto (x_0/x)^{\lambda(Q^2)}$ . Due to an increase in  $\lambda(Q^2)$  with  $Q^2$ , the drop of the amplitude due to a decrease in the dipole size is compensated to some extent by a faster increase in the gluon density. Thus,  $x_{cr}$  at which unitarity breaks down, increases with an increase in  $Q^2$  rather slowly.

A similar conflict with probability conservation exists for the perturbative "Pomeron". The energy at which this conflict becomes acute obviously depends on the impact parameter, see [130] and references therein. Note also that the conflict with unitarity exists not only for scattering of small dipoles off hadrons, but also in the case of scattering of two small objects [133].

### 8.3 Gluon dipole–proton scattering at the upper edge of HERA kinematics

To demonstrate that the new QCD regime for a gluon cloud is not far from the kinematical domain probed at the LHC, we consider here scattering of a colorless small gluon dipole off the nucleon (for a detailed discussion, see [134]). One can evaluate  $\Gamma_{gg}(x, b)$  based on the information on the total cross section of the  $q\bar{q}$  dipole–nucleon interaction extracted from DIS inclusive data (Eq. 65), the  $t$  dependence of the two-gluon form factor (section 7), and the relation

$$\Gamma_{gg}^{\text{inel}}(x, b) = \frac{9}{4} \Gamma_{q\bar{q}}^{\text{inel}}(x, b). \quad (119)$$

The knowledge of  $\Gamma_{gg}(x, b)$  allows us to calculate the total and elastic cross sections of the colorless "gluon–gluon" dipole–nucleon scattering. (By definition, the imaginary part of the partial wave for the dipole–nucleon scattering is  $\Gamma_{gg}(x, b)$ .) The ratio of the elastic and total cross sections for the scattering of a color-singlet dipole off the nucleon is:

$$R_g(x, Q^2) = \frac{\int d^2b |\Gamma_{gg}(b)|^2}{2 \int d^2b \Gamma_{gg}(b)}. \quad (120)$$

Numerical estimates [134] indicate that for  $d = 0.1$  fm ( $Q^2 \sim 40$  GeV<sup>2</sup>) corresponding to  $\Upsilon$  photoproduction, the value of  $R_g(x, Q^2)$  is small ( $\sim 0.14$ )

for  $x \sim 10^{-4}$ . However,  $R_g(x, Q^2)$  reaches the value of  $\sim 0.4$ , when  $x$  goes down to  $10^{-7}$  indicating that for such  $x$ , most of the cross section maybe due to the interaction in the BDR. At the same time, for  $Q^2 \sim 4 \text{ GeV}^2$  one finds that the interaction is nearly black over a rather large range of impact parameters already for  $x \sim 10^{-4}$ , leading to  $R_g \sim 0.3 - 0.4$ . At the same time, in the  $q\bar{q}$ -nucleon case, significantly smaller  $x$  are necessary to reach the BDR. So the interaction in this channel is rather far from the regime of complete absorption at  $x$  achieved at HERA.

The predictions discussed above can be compared with the experimental data on diffraction in DIS obtained at HERA. The sum of the cross sections of color-singlet gluon dipole elastic scattering and of inelastic diffraction scattering is calculable in terms of diffractive gluon PDFs (when an external hard probe couples directly to the gluon) integrated over the momentum of the diffracted proton with the cut  $x_{\mathbb{P}} \leq 0.03$ . The total cross section of the color singlet dipole-proton scattering is calculable in terms of the gluon density of the nucleon. Thus, to compare  $R_g$  with the data, one should measure the ratio of the diffractive and inclusive cross sections induced by a hard probe coupled to gluons:

$$R_g(x, Q^2) = \frac{\int_x^{0.03} dx_{\mathbb{P}} \int_0^{-\infty} dt f_g^{D(4)}(x/x_{\mathbb{P}}, Q^2, x_{\mathbb{P}}, t)}{g_N(x, Q^2)}, \quad (121)$$

where  $f_g^{D(4)}$  is the diffractive gluon PDF. It can be evaluated using the most recent analyses of hard diffraction at HERA. One finds that  $R_g(x \sim 10^{-4}, Q^2 = 4 \text{ GeV}^2) \sim 0.3$  and  $R_q(x \sim 10^{-4}, Q^2 = 4 \text{ GeV}^2) \sim 0.2$  which confirms proximity of the gluon interaction to the BDR at small impact parameters (for the recent update, see Fig. 69 in [135]).

A word of caution is necessary here. These calculations are based on the leading log approximation where such higher order Fock states as  $q\bar{q}g$  are neglected. Hence, these calculation should only be considered as semi-quantitative ones.

## 8.4 The regime of complete absorption

Bjorken scaling, i.e., the dependence of cross sections of hard processes only on the hard scale, completely disappears in the black-disc regime only for a specific range of  $Q^2$  that depends on  $x$ . Basic formulas of the black-disc regime for the total cross section of photo(electro)production of hadrons off

a heavy nucleus at high energies were derived by V. Gribov [136] by analyzing the contribution of diffraction to the structure functions of heavy nuclei and an increase in absorption with an increase in the atomic number. The theoretical observation that enabled the calculation was that in the BDR, non-diagonal transitions between diffractively produced hadronic states are absent at zero angles.

Interesting features of this regime include the dominance of diffraction into dijets which constitutes 50% of the total cross section, a gross change of the  $Q^2$  dependence of exclusive meson production (from  $1/Q^6$  to  $1/Q^2$  for the case of the longitudinal photon), and gross suppression of leading hadron production in the current fragmentation region (suppression of the effective fractional energy losses) [128].

A big challenge is to establish the mechanism of the onset of the BDR and the basic features of the BDR. A popular approach is to tame the rapid increase in the perturbative LO "Pomeron" with energy by taking into account the simplest non-linear effects [137]. This approach has even more severe problems as compared to the perturbative "Pomeron". Indeed, energy-momentum conservation restricts the number of allowed branchings of the "Pomerons" due to the triple "Pomeron" and the number of multi-"Pomeron" exchanges. The restriction follows from the fact that an exchange of the perturbative "Pomeron" is dominated by inelastic processes which carry energy and momentum. This restriction is especially severe for the multi-Regge kinematics explored in [137]. Thus, the contribution of fan diagrams relevant in this approach for the screening of the perturbative "Pomeron" requires collision energies that cannot be treated in a realistic way at the collider energies.

The appearance of new scales in addition to  $Q^2$  follows from the fact that the decomposition over twists becomes meaningless at sufficiently small  $x$  since the decomposition parameter starts to exceed the radius of convergence. As a result, an analytic continuation becomes necessary.

The new scale depends on the incident energy as a result of probability conservation. This property of the new QCD regime distinguishes it from the pQCD regime. It may indicate that in this regime, violation of the two-dimensional translation symmetry, or even conformal invariance, takes place. This option has been suggested for soft processes in [138, 139] and for hard QCD in [129]. In this case, the quasi-Goldstone mode is the motion along the impact parameter in the region of complete absorption. Moreover it is unclear whether pQCD is applicable even qualitatively for the description of the new QCD regime since in the kinematics where the interaction becomes

strong, one should take into account the Gribov copies found in [140].

## 9 Conclusions

The theory of the  $S$ -matrix allowed one to understand many regularities of diffractive processes in the regime that is now referred to as the soft QCD regime. Further progress became possible with an advent of QCD and the focus on the processes involving a hard scale.

Investigations of diffractive phenomena led to the ideas, concepts, and technologies of the calculations that form the foundation of modern particle physics and are the basis for the future developments aiming at bridging the gap between soft and hard phenomena. The exploration of the color transparency phenomenon supplies a new method of investigations of hadrons and nuclei. Investigation of the new QCD regime of strong interaction will allow one to find new phenomena and to develop new methods of treating phase transitions in the relativistic kinematics. The long-standing challenges include confinement of quarks and gluons and spontaneously broken chiral symmetry.

Also, QCD is the only quantum field theory leading to non-linear phenomena that can be probed in laboratory. Hence, it may provide new tools for developing a theory beyond the Standard Model of strong and electroweak interactions.

## 10 Acknowledgments

We thank J. Bjorken, V. N. Gribov and A. H. Mueller for the illuminating discussions of diffractive phenomena in high energy processes. We thank V. Guzey for reading manuscript and valuable comments. The research was supported by DOE and BSF.

## References

- [1] L.D. Landau, Talk at Kiev conference 1959, published in, Theoretical physics in the 20th century: A memorial volume to W Pauli, p. 245 (Eds M Fierz, V F Weisskopf) (New York: Interscience Publishers, 1960).

- [2] H. Lehmann, K. Symanzik and W. Zimmermann, *Nuovo Cim.* **6** (1957) 319.
- [3] L. D. Landau, *Nucl. Phys.* **13** (1959) 181.
- [4] S. Mandelstam, *Phys. Rev.* **112** (1958) 1344.
- [5] G. F. Chew, S. C. Frautschi and S. Mandelstam, *Phys. Rev.* **126** (1961) 1202.
- [6] R. J. Eden, P. V. Landshoff, D. I. Olive, "Analytic S- matrix"  
*Cambridge Univ. Pr. (2002) 296*
- [7] M. Froissart, *Phys. Rev.* **123** (1961) 1053.
- [8] V. N. Gribov, *Sov. Phys. JETP* **14** (1962) 1395 [*Zh. Eksp. Teor. Fiz.* **41** (1961) 1962].  
M.Froissart, Report to the La Jolla Conference on the Theory of Weak and Strong Interactions, La Jolla,1961(unpublished)
- [9] T. Regge, *Nuovo Cim.* **14** (1959) 951; **18** (1960) 947.
- [10] Cited in S. C. Frautschi, M. Gell-Mann, and F. Zahariasen, *Phys.Rev.* **126** (1962) 2204.
- [11] V. N. Gribov, *Sov. Phys. JETP* **15** (1962) 873 [*Zh. Eksp. Teor. Fiz.* **42** (1962) 1260] [*Nucl. Phys.* **40** (1963) 107].
- [12] V. N. Gribov and I. Y. Pomeranchuk, *Sov. Phys. JETP* **15** (1962) 788L [*Zh. Eksp. Teor. Fiz.* **42** (1962) 1141] [*Phys. Rev. Lett.* **8** (1962) 343].
- [13] G. F. Chew and S. C. Frautschi, *Phys. Rev. Lett.* **8** (1962) 41.
- [14] V. N. Gribov, I. Ya. Pomeranchuk and K. A. Ter-Martirosian, *Phys. Lett.* **9** (1964) 269.
- [15] V. N. Gribov, *Nucl. Phys.* **22** (1961) 249; *Zh. Eksp. Teor. Fiz.* **41** (1961) 667 [*Sov. Phys. JETP* **14** (1962) 478 ].
- [16] A. C. Irving and R. P. Worden, *Phys. Rept.* **34** (1977) 117.
- [17] V. N. Gribov, "The theory of complex angular momenta: Gribov lectures on theoretical physics," *Cambridge Univ. Pr. (2003) 297 p*

- [18] M. Gell-Mann, M. L. Goldberger, F. E. Low, V. Singh and F. Zachari-  
 asen, Phys. Rev. **133**, B161 (1964).
- [19] L. L. Frankfurt and V. E. Sherman, Sov. J. Nucl. Phys. **23** (1976) 581.  
 L.N. Lipatov Sov. J. Nucl. Phys. **23** (1976) 338.
- [20] V. S. Fadin and V. E. Sherman, Pisma Zh. Eksp. Teor. Fiz. **23** (1976)  
 599.
- [21] R. Dolen, D. Horn and C. Schmid, Phys. Rev. **166** (1968) 1768.
- [22] G. F. Chew and S. C. Frautschi, Phys. Rev. Lett. **7** (1961) 394.
- [23] M. Strikman, Nucl. Phys. A **805** (2008) 369 [arXiv:0711.1634 [hep-ph]].
- [24] L.L.Frankfurt and V. A.Khose Materials of 10 Winter School on nuclear  
 and particle physics,v. — Leningrad 1975, pp 196-408.
- [25] I. Ya. Pomeranchuk, JETP, **34** (1958) 725.
- [26] V. N. Gribov, JETP Lett. **41** (1961) 667-669;
- [27] V. N. Gribov and I. Y. .Pomeranchuk, Sov. Phys. JETP **16** (1963) 220  
 [Zh. Eksp. Teor. Fiz. **43** (1962) 308] [Nucl. Phys. **38** (1962) 516].
- [28] P. V. Landshoff, Acta Phys. Polon. B **40** (2009) 1967 [arXiv:0903.1523  
 [hep-ph]].
- [29] A. Levy, arXiv:0711.0737 [hep-ex].
- [30] B. List [H1 Collaboration], arXiv:0906.4945 [hep-ex].
- [31] G. Antcheva et al [The TOTEM collaboration], TOTEM 2012-002.
- [32] M. Block and R. N. Cahn, Rev. Mod. Phys. **57** (1985) 563.
- [33] B. Blok, L. Frankfurt and M. Strikman, Eur. Phys. J. C **67** (2010) 99  
 [arXiv:1001.2469 [hep-ph]].
- [34] ibitemBrodsky:1994kf S. J. Brodsky, L. Frankfurt, J. F. Gunion,  
 A. H. Mueller and M. Strikman, Phys. Rev. D **50** (1994) 3134 [hep-  
 ph/9402283].

- [35] O. V. Kancheli, JETP Lett. **11** (1970) 267 [Pisma Zh. Eksp. Teor. Fiz. **11** (1970) 397].
- [36] A. H. Mueller, Phys. Rev. D **4** (1971) 150.
- [37] CDF Collaboration, Phys. Rev. **D50** (1994) 5535.
- [38] G. Aad *et al.* [ATLAS Collaboration], Eur. Phys. J. C **72** (2012) 1926 [arXiv:1201.2808 [hep-ex]].  
B. Abelev *et al.* [The ALICE Collaboration], arXiv:1208.4968 [hep-ex].
- [39] V. A. Abramovsky, V. N. Gribov and O. V. Kancheli, Yad. Fiz. **18** (1973) 595 [Sov. J. Nucl. Phys. **18** (1974) 308].
- [40] V. N. Gribov, I. Y. Pomeranchuk and K. A. Ter-Martirosian, Phys. Rev. **139** (1965) B184.
- [41] S. Mandelstam, Nuovo Cim. **30** (1963) 1148.
- [42] V. N. Gribov, Sov. Phys. JETP **26** (1968) 414 [Zh. Eksp. Teor. Fiz. **53** (1967) 654].
- [43] V. N. Gribov and A. A. Migdal, Zh. Eksp. Teor. Fiz. **55** (1968) 4.
- [44] V. N. Gribov, Sov. J. Nucl. Phys. **9** (1969) 246
- [45] R. P. Feynman, "Photon-hadron interactions," W.A. Benjamin, Inc, Reading, Massachusetts, 1972, 282p
- [46] G. Fidecaro, M. Fidecaro, L. Lanceri, S. Nurushev, L. Piemontese, V. Solovyanov, A. Vascotto and F. Gasparini *et al.*, Phys. Lett. B **105** (1981) 309.
- [47] V. A. Abramovsky and R. G. Betman, Sov. J. Nucl. Phys. **55** (1992) 912.
- [48] L. D. Landau, E. M. Lifshitz, Quantum Mechanics Non-Relativistic Theory, Third Edition: Volume 3, Pergamon Press, 1977.
- [49] A. Martin, Phys. Rev. **129** (1963) 1432;



- [50] L. D. Landau and I. Ya. Pomeranchuk, Dokl. Akad. Nauk SSSR **92** (1953) 535, 735.  
M.L. Ter-Mikaelian, Dokl. Akad. Nauk SSSR **94** (1954) 1033  
A. B. Migdal, Phys. Rev. **103** (1956) 1811.  
M.L. Ter-Mikaelian, High Energy Electromagnetic Processes in Condensed Media, John Wiley & Sons, NY, 1972.
- [51] V. N. Gribov, B. L. Ioffe and I. Y. Pomeranchuk, Sov. J. Nucl. Phys. **2** (1966) 549 [Yad. Fiz. **2** (1965) 768].
- [52] V.N. Gribov. In \*Moscow 1 ITEP school, v.1 'Elementary particles'\*, 65,1973, hep-ph/0006158.
- [53] B. Blok and L. Frankfurt, Phys. Rev. D **75** (2007) 074001 [hep-ph/0611062].
- [54] . V. N. Gribov, Sov. Phys. JETP **29** (1969) 483 [Zh. Eksp. Teor. Fiz. **56** (1969) 892].
- [55] V. A. Karmanov and L. A. Kondratyuk, Pisma Zh. Eksp. Teor. Fiz. **18** (1973) 451.
- [56] J. C. Collins, L. Frankfurt and M. Strikman, Phys. Rev. D **56** (1997) 2982 [hep-ph/9611433].
- [57] D. Dutta and K. Hafidi, Int. J. Mod. Phys. E **21** (2012) 1230004 [arXiv:1209.5295 [nucl-ex]].
- [58] F. E. Low, Phys. Rev. D **12** (1975) 163.
- [59] S. Nussinov, Phys. Rev. Lett. **34** (1975) 1286.
- [60] J. F. Gunion and D. E. Soper, Phys. Rev. D **15** (1977) 2617.
- [61] B. Blaettel, G. Baym, L. L. Frankfurt and M. Strikman, Phys. Rev. Lett. **70** (1993) 896.
- [62] L. Frankfurt, G. A. Miller and M. Strikman, Phys. Lett. B **304** (1993) 1 [hep-ph/9305228].

- [63] L. Frankfurt, A. Radyushkin and M. Strikman, Phys. Rev. D **55** (1997) 98 [hep-ph/9610274].
- [64] A. H. Mueller, Nucl. Phys. B **335** (1990) 115.
- [65] G. V. Frolov, V. N. Gribov and L. N. Lipatov, Phys. Lett. B **31** (1970) 34.  
V. N. Gribov, L. N. Lipatov and G. V. Frolov, Sov. J. Nucl. Phys. **12** (1971) 543 [Yad. Fiz. **12** (1970) 994].
- [66] E. A. Kuraev, L. N. Lipatov and V. S. Fadin, Sov. Phys. JETP **45** (1977) 199 [Zh. Eksp. Teor. Fiz. **72** (1977) 377].  
I. I. Balitsky and L. N. Lipatov, Sov. J. Nucl. Phys. **28** (1978) 822 [Yad. Fiz. **28** (1978) 1597].
- [67] A. H. Mueller, Nucl. Phys. B **415** (1994) 373.  
Z. Chen and A. H. Mueller, Nucl. Phys. B **451** (1995) 579.
- [68] A. H. Mueller, Phys. Lett. B **396** (1997) 251 [hep-ph/9612251].
- [69] M. Ciafaloni, M. Taiuti and A. H. Mueller, Nucl. Phys. B **616** (2001) 349 [hep-ph/0107009].
- [70] M. Ciafaloni and D. Colferai, Phys. Lett. B **452** (1999) 372 [hep-ph/9812366].
- [71] V. S. Fadin and L. N. Lipatov, Phys. Lett. B **429** (1998) 127 [hep-ph/9802290].
- [72] E. A. Kuraev and L. N. Lipatov, Yad. Fiz. **16** (1972)1060 [Sov. J. Nucl. Phys. **16** (1973) 584]
- [73] G. Altarelli, R. D. Ball and S. Forte, Nucl. Phys. B **575** (2000) 313 [hep-ph/9911273].
- [74] M. Ciafaloni, D. Colferai, G. P. Salam and A. M. Stasto, Phys. Rev. D **68** (2003) 114003.
- [75] H. I. Miettinen and J. Pumplin, Phys. Rev. D **18** (1978) 1696.

- [76] B. Blaettel, G. Baym, L. L. Frankfurt, H. Heiselberg and M. Strikman, Phys. Rev. D **47** (1993) 2761.
- [77] M. L. Good and W. D. Walker, Phys. Rev. **120** (1960) 1857.
- [78] B. Z. Kopeliovich and L. I. Lapidus, Pisma Zh. Eksp. Teor. Fiz. **28** (1978) 664.
- [79] L. Frankfurt, G. A. Miller and M. Strikman, Phys. Rev. Lett. **71** (1993) 2859 [hep-ph/9309285].
- [80] M. Strikman and V. Guzey, Phys. Rev. C **52** (1995) 1189 [nucl-th/9506010].
- [81] L. Frankfurt, V. Guzey and M. Strikman, J. Phys. G G **27** (2001) R23 [hep-ph/0010248].
- [82] G. Baym, B. Blattel, L. L. Frankfurt, H. Heiselberg and M. Strikman, Phys. Rev. C **52** (1995) 1604 [nucl-th/9502038].
- [83] F. D. Aaron *et al.* [H1 and ZEUS Collaborations], arXiv:1207.4864 [hep-ex].
- [84] J. C. Collins, Phys. Rev. D **57** (1998) 3051 [Erratum-ibid. D **61** (2000) 019902] [hep-ph/9709499].
- [85] J. D. Bjorken, Conf. Proc. C **710823** (1971) 281.  
J. D. Bjorken and J. B. Kogut, Phys. Rev. D **8** (1973) 1341.
- [86] J. D. Bjorken, Lect. Notes Phys. **56** (1976) 93.
- [87] L. L. Frankfurt and M. Strikman, Phys. Rep. **160** (1988) 235-427.
- [88] H. Abramowicz, L. Frankfurt and M. Strikman, eConf C **940808** (1994) 033 [Surveys High Energ. Phys. **11** (1997) 51]
- [89] H. Kowalski, T. Lappi, C. Marquet and R. Venugopalan, Phys. Rev. C **78** (2008) 045201 [arXiv:0805.4071 [hep-ph]].
- [90] J. Bartels and M. Loewe, Z. Phys. C **12** (1982) 263.
- [91] I. I. Balitsky and V. M. Braun, Nucl. Phys. B **311** (1989) 541.

- [92] D. Mueller, D. Robaschik, B. Geyer, F. M. Dittes and J. Horejsi, Fortsch. Phys. **42** (1994) 101 [hep-ph/9812448].
- [93] X. -D. Ji, Phys. Rev. Lett. **78** (1997) 610 [hep-ph/9603249]; Phys. Rev. D **55** (1997) 7114 [hep-ph/9609381].
- [94] A. V. Radyushkin, Phys. Lett. B **380** (1996) 417 [hep-ph/9604317]; Phys. Rev. D **56** (1997) 5524 [hep-ph/9704207].
- [95] X. -D. Ji, J. Phys. G **24** (1998) 1181 [hep-ph/9807358].
- [96] L. L. Frankfurt, A. Freund and M. Strikman, Phys. Rev. D **58** (1998) 114001 [Erratum-ibid. D **59** (1999) 119901] [hep-ph/9710356].
- [97] M. Diehl, T. Gousset, B. Pire and O. Teryaev, Phys. Rev. Lett. **81** (1998) 1782 [hep-ph/9805380].
- [98] L. L. Frankfurt, P. V. Pobylitsa, M. V. Polyakov and M. Strikman, Phys. Rev. D **60** (1999) 014010 [hep-ph/9901429].
- [99] A. V. Radyushkin, Phys. Lett. B **385** (1996) 333 [hep-ph/9605431].
- [100] L. Frankfurt, A. Freund, V. Guzey and M. Strikman, Phys. Lett. B **418** (1998) 345 [Erratum-ibid. B **429** (1998) 414] [hep-ph/9703449].
- [101] A. G. Shuvaev, K. J. Golec-Biernat, A. D. Martin and M. G. Ryskin, Phys. Rev. D **60** (1999) 014015 [hep-ph/9902410].
- [102] M. G. Ryskin, Z. Phys. C **57** (1993) 89.
- [103] L. Frankfurt, W. Koepf and M. Strikman, Phys. Rev. D **54** (1996) 3194 [hep-ph/9509311]; Phys. Rev. D **57** (1998) 512 [hep-ph/9702216].
- [104] A. J. Baltz, G. Baur, D. d'Enterria, L. Frankfurt, F. Gelis, V. Guzey, K. Hencken, (ed.) and Y. .Kharlov *et al.*, Phys. Rept. **458** (2008) 1 [arXiv:0706.3356 [nucl-ex]].
- [105] L. L. Frankfurt, M. F. McDermott and M. Strikman, JHEP **9902** (1999) 002 [hep-ph/9812316].
- [106] A. D. Martin, M. G. Ryskin and T. Teubner, Phys. Lett. B **454** (1999) 339 [hep-ph/9901420].

- [107] S. Chekanov *et al.* [ZEUS Collaboration], Nucl. Phys. B **695** (2004) 3 [hep-ex/0404008].
- [108] S. Chekanov *et al.* [ZEUS Collaboration], PMC Phys. A **1** (2007) 6 [arXiv:0708.1478 [hep-ex]].
- [109] L. Mankiewicz and G. Piller, Phys. Rev. D **61** (2000) 074013
- [110] K. Goeke, M. V. Polyakov and M. Vanderhaeghen, Prog. Part. Nucl. Phys. **47** (2001) 401
- [111] A. Freund and M. F. McDermott, Phys. Rev. D **65** (2002) 091901
- [112] M. Strikman and C. Weiss, Phys. Rev. D **69** (2004) 054012 [hep-ph/0308191].
- [113] L. Frankfurt, M. Strikman and C. Weiss, Phys. Rev. D **83** (2011) 054012 [arXiv:1009.2559 [hep-ph]].
- [114] L. Frankfurt and M. Strikman, Phys. Rev. D **66** (2002) 031502 [hep-ph/0205223].
- [115] L. Frankfurt, M. Strikman, D. Treleani and C. Weiss, Phys. Rev. Lett. **101** (2008) 202003 [arXiv:0808.0182 [hep-ph]].
- [116] L. Frankfurt and M. Strikman, Phys. Rev. Lett. **63** (1989) 1914 [Erratum-ibid. **64** (1990) 815].
- [117] S. Chekanov *et al.* [ZEUS Collaboration], Nucl. Phys. B **695** (2004) 3 [arXiv:hep-ex/0404008];  
A. Aktas *et al.* [H1 Collaboration], Eur. Phys. J. C **46** (2006) 585 [arXiv:hep-ex/0510016].
- [118] L. Frankfurt, G. A. Miller and M. Strikman, Phys. Rev. D **65**, 094015 (2002) [arXiv:hep-ph/0010297].
- [119] E. M. Aitala *et al.* [E791 Collaboration], *Phys. Rev. Lett.* **86**, 4768 (2001), *ibid* **86**, 4773 (2001).
- [120] V. M. Braun, D. Y. Ivanov, A. Schafer and L. Szymanowski, Phys. Lett. B **509** (2001) 43; Nucl. Phys. B **638** (2002) 111

- [121] M. D. Sokoloff *et al.* Phys. Rev. Lett. **57**, 3003 (1986).
- [122] L. Frankfurt, G. Piller, M. Sargsian and M. Strikman, Eur. Phys. J. A **2** (1998) 301 [nucl-th/9801041].
- [123] G. R. Farrar, H. Liu, L. L. Frankfurt and M. I. Strikman, Phys. Rev. Lett. **61** (1988) 686.
- [124] M. R. Adams *et al.* (E665), Phys. Rev. Lett. **74**, 1525 (1995).
- [125] A. Airapetian *et al.* (HERMES), Phys. Rev. Lett. **90**, 052501 (2003).
- [126] B. Clasie *et al.*, Phys. Rev. Lett. **99**, 242502 (2007).
- [127] L. El Fassi, L. Zana, K. Hafidi, M. Holtrop, B. Mustapha, W. K. Brooks, H. Hakobyan and X. Zheng *et al.*, Phys. Lett. **B 712**, 326 (2012).
- [128] L. Frankfurt, V. Guzey, M. McDermott and M. Strikman, Phys. Rev. Lett. **87** (2001) 192301 [hep-ph/0104154].
- [129] B. Blok and L. Frankfurt, Phys. Rev. D **73** (2006) 054008 [hep-ph/0508218].
- [130] G. Watt and H. Kowalski, Phys. Rev. D **78** (2008) 014016 [arXiv:0712.2670 [hep-ph]].
- [131] S. Munier, A. M. Stasto and A. H. Mueller, Nucl. Phys. B **603** (2001) 427 [hep-ph/0102291].
- [132] T. Rogers, V. Guzey, M. Strikman and X. Zu, Phys. Rev. D **69** (2004) 074011. [hep-ph/0309099].
- [133] A. H. Mueller, Nucl.Phys.B437:107-126,1995.
- [134] L. Frankfurt, T. Rogers, M. Strikman, in preparation.
- [135] L. Frankfurt, V. Guzey and M. Strikman, Phys. Rept. **512** (2012) 255 [arXiv:1106.2091 [hep-ph]].
- [136] V. N. Gribov, Sov. Phys. JETP **30** (1970) 709 [Zh. Eksp. Teor. Fiz. **57** (1969) 1306].

- [137] I. Balitsky, Nucl. Phys. B **463** (1996) 99 [hep-ph/9509348].  
Y. V. Kovchegov, Phys. Rev. D **61** (2000) 074018 [hep-ph/9905214].
- [138] D. Amati, G. Marchesini, M. Ciafaloni and G. Parisi, Nucl. Phys. B **114** (1976) 483.
- [139] D. Amati, M. Le Bellac, G. Marchesini and M. Ciafaloni, Nucl. Phys. B **112** (1976) 107.
- [140] V. N. Gribov, Nucl. Phys. B **139** (1978) 1.